The variational collocation method

Hector Gomez[a,*], Laura De Lorenzis[b]

[a]*Departamento de Métodos Matemáticos, Universidade da Coruña, Campus de A Coruña, 15071, A Coruña, Spain.*
[b]*Institut für Angewandte Mechanik, Technische Universität Braunschweig, Bienroder Weg 87, 38106 Braunschweig, Germany*

Abstract

We propose the *variational collocation method* for the numerical solution of partial differential equations. The conceptual basis is the establishment of a direct connection between the Galerkin method and the classical collocation methods, with the perspective of achieving the accuracy of the former with a computational cost of one point evaluation per degree of freedom as in the latter. Variational collocation requires a discrete space constructed by smooth and pointwise non-negative basis functions, which makes the approach immediately applicable to isogeometric analysis and some meshfree methods. In this paper, we concentrate on isogeometric analysis and demonstrate that there exists a set of points such that collocation of the strong form at these points produces the Galerkin solution exactly. We provide an estimate of these points and show that applying isogeometric collocation at the estimated points completely solves the well-known odd/even discrepancy in the order of spatial convergence. We demonstrate the potential of variational collocation with examples of linear and non-linear elasticity as well as Kirchhoff plates.

Keywords: Variational collocation, Isogeometric analysis, Galerkin method, Collocation method, Meshfree method

1. Introduction

The most widely used approach to solve partial differential equations (PDEs) in computational mechanics is the finite element method, which is normally applied to a weak form of the PDE of interest. The first step to derive the weak form is to multiply the strong form of the governing differential equation with a weight function and integrate over the computational domain, which leads to the so-called weighted residual formulation. For standard second-order problems of fluid and solid mechanics, the weak formulation is an alternative weighted residual formulation, which is obtained through integration by parts. An approach of particular interest is the Galerkin method, obtained by defining a suitable discrete space where the solution is sought, and adopting (in the most used Bubnov-Galerkin

*Corresponding author.
Email address: hgomez@udc.es (Hector Gomez)

approach) the same space for the weighting functions. Following the standard convention, we will also refer to finite element schemes as variational methods.

Collocation methods are an alternative approach in which the strong form of the PDE is enforced at a set of sites called collocation points[1]. A simple way to derive a collocation method from a weak form is to counter-integrate by parts to obtain the weighted residual formulation of the strong form and replace the weight functions with Dirac delta distributions centered at collocation points. Note that this argument requires additional smoothness to that needed for the weak form to be well posed, and that all the properties of the Galerkin method may be lost in the process. The advantage is that collocation methods are faster than variational methods on a per degree of freedom basis, as the computation of the residual and the tangent matrix requires only one point evaluation per unknown. Thus, collocation methods could be also thought of as stable one-point quadratures. The advantages of collocation are particularly evident in applications where the efficiency is directly related to the cost of quadrature, such as in explicit structural dynamics, where the computational cost is dominated by stress divergence evaluations at quadrature points for the calculation of the residual force vector.

The above-mentioned requirement of additional smoothness has been a significant obstacle for the development of collocation methods in the finite element community (primarily dominated by second-order PDEs) because classical Lagrangian finite elements are only $\mathcal{C}^0$-continuous at the element boundaries. Some noteworthy exceptions are based on spectral finite elements [1, 2], but there has also been recent work that accounts directly for the jumps in the derivatives at the element boundaries using classical $\mathcal{C}^0$ finite elements [3]. Another important development has been the recent appearance of isogeometric analysis (IGA), a spline-based finite element method which uses smooth basis functions commonly employed in Computer Aided Design (CAD) [4, 5, 6]. The higher-order continuity of the basis functions used in IGA (among other advantages [7, 8, 9, 10]) allows for a straightforward application of the collocation method, while retaining the geometric flexibility of finite elements [11, 12, 13]. Isogeometric collocation has recently triggered a great interest in the computational mechanics community [14, 15, 16, 17, 18]. Recent results suggest that collocation may perform better than Galerkin in terms of accuracy per unit of computing time [19]. Conversely, its accuracy per degree of freedom is significantly lower than that of the Galerkin method, especially when odd interpolation degrees are adopted. In particular, the order of spatial convergence (measured, e.g., in elasticity in the $\mathcal{L}^2$ norm of the displacement error) for isogeometric collocation performed at the so-called Greville or Demko abscissae is equal to p for even and $p-1$ for odd degrees [11, 12].

In this work, we make use of suitable mathematical tools to establish a direct connection between the Galerkin method and the classical collocation methods, with the perspective of achieving the accuracy of the former with a computational cost of one point evaluation per degree of freedom as in the latter, in other words, with the perspective of achieving

[1]Boundary conditions are also imposed at a set of points, but we do not consider them here to simplify the discussion.

the advantages of both *simultaneously*. We refer to this approach as *variational collocation*. We demonstrate that, for discrete spaces constructed with sufficiently smooth and pointwise non-negative basis functions, there exists a set of points such that collocation at these sites produces the Galerkin solution *exactly*. For reasons that will be clear later, we denote these collocation sites *Cauchy-Galerkin points*. The aforementioned prerequisites on the basis functions make the variational collocation approach naturally applicable to isogeometric analysis and some meshfree methods, e.g., maximum entropy schemes [23]. In this paper, we concentrate on isogeometric analysis. We prove mathematically and verify numerically that isogeometric collocation at Cauchy-Galerkin points produces the Galerkin solution *exactly*. We then provide an *estimate* of these points and show that applying isogeometric collocation at the estimated Cauchy-Galerkin points rather than at the traditional Greville or Demko abscissae completely solves the aforementioned odd/even discrepancy, guaranteeing a convergence order of p for all interpolation degrees and thus significantly raising the accuracy for splines of odd degree. A striking result of our analysis is that the Greville and Demko abscissae are the worst possible choice for splines of odd degree. We demonstrate the potential of variational collocation with examples of linear and non-linear elasticity as well as Kirchhoff plates.

In the main application framework of the current paper, i.e., isogeometric analysis, variational collocation may be regarded as isogeometric collocation at Cauchy-Galerkin points (or, to be more precise, at their estimates). However, the conceptual basis and the potential scope of variational collocation are much wider. In this paper, we briefly explore potential opportunities related to reduced quadrature schemes. Moreover, we expect variational collocation to have an impact not only on IGA, but also on other fields of computational mechanics where smooth and non-negative basis functions are used, e.g., in some meshfree methods, most notably in maximum entropy schemes.

The outline of the rest of the paper is as follows: Sect. 2 illustrates the idea of variational collocation. Sect. 3 focuses on the application of variational collocation to isogeometric analysis and proves that collocation at Cauchy-Galerkin points produces the Galerkin solution exactly. This result is corroborated numerically in Sect. 4, where we also give an estimate of the location of Cauchy-Galerkin points for isogeometric collocation. Sect. 5 illustrates the performance of our method with some numerical examples involving linear and non-linear elasticity as well as Kirchhoff plates. We explore potential opportunities opened by the concept of variational collocation in Sect. 6 and close with conclusions in Sect. 7.

2. The idea of variational collocation

Although the idea behind the variational collocation method is valid for any PDE with smooth solution, we illustrate the fundamental concepts using a simple boundary value problem defined by the Poisson equation. Let $\Omega \subset \mathbb{R}^d$ be an open set representing the problem domain, where d is the number of spatial dimensions. The boundary of Ω, denoted by Γ, is assumed to be smooth. The problem can be stated in strong form as follows: Given

$f : \Omega \mapsto \mathbb{R}$ and $u_D : \Gamma \mapsto \mathbb{R}$, find $u : \Omega \mapsto \mathbb{R}$ such that

$$\Delta u + f = 0 \quad \text{in} \quad \Omega \tag{1}$$
$$u = u_D \qquad \text{on} \quad \Gamma \tag{2}$$

In what follows, we first outline the differences between classical variational and collocation schemes, and then introduce the idea of variational collocation.

2.1. Variational versus collocation methods

We compare variational and collocation methods by discretizing the boundary value problem (1)–(2) using both methodologies.

2.1.1. Variational method

Let us consider trial and weighting function spaces defined, respectively, as

$$\mathcal{U} = \{u \mid u \in \mathcal{H}^1,\ u = u_D \ \text{ on } \ \Gamma\} \tag{3}$$
$$\mathcal{W} = \{w \mid w \in \mathcal{H}^1,\ w = 0 \ \text{ on } \ \Gamma\} \tag{4}$$

where $\mathcal{H}^1$ is the Sobolev space of square integrable functions with square integrable first derivatives. The Poisson problem (1)–(2) may be rewritten in weak form as: Given $f : \Omega \mapsto \mathbb{R}$, find $u \in \mathcal{U}$, such that for all $w \in \mathcal{W}$

$$\int_\Omega \nabla w \cdot \nabla u \, \mathrm{d}x - \int_\Omega w f \, \mathrm{d}x = 0 \tag{5}$$

To perform space discretization, we define a finite-dimensional space $\mathcal{U}_h = \text{span}\{N_A\}_{A=1,\dots,n}$. Here, the N_A's are linearly independent basis functions and, as a consequence, $\dim(\mathcal{U}_h) = n$. Let us call $\mathcal{D}$ the set of indices A such that N_A vanishes on Γ. The complementary set of indices is called $\mathcal{B}$, therefore the functions $\{N_A\}_{A\in\mathcal{B}}$ do not vanish on Γ. We define $\mathcal{W}^h \subset \mathcal{W}$ as $\mathcal{W}^h = \text{span}\{N_A\}_{A\in\mathcal{D}}$, which leads to a Galerkin formulation. Then, the discretization of Eq. (5) may be written as: Given $f : \Omega \mapsto \mathbb{R}$, find $u_h \in \mathcal{U}_h$ such that

$$\int_\Omega \nabla N_A \cdot \nabla u_h \, \mathrm{d}x - \int_\Omega N_A f \, \mathrm{d}x = 0 \quad \text{for all} \quad A \in \mathcal{D} \tag{6}$$

Note that Eq. (6) is imposed only for the N_A's for which $A \in \mathcal{D}$. The remaining functions in $\mathcal{U}_h$, that is, $\{N_A\}_{A\in\mathcal{B}}$, are used to impose the Dirichlet boundary conditions strongly. If we express u_h as a linear combination of the basis functions, i.e.,

$$u_h(\boldsymbol{x}) = \sum_{B=1}^{n} u_B N_B(\boldsymbol{x}), \tag{7}$$

then, Eq. (6), along with the constraints that impose Dirichlet boundary conditions strongly, constitute a linear system of equations that allows us to compute u_h and obtain the Galerkin solution to the problem.

2.1.2. Collocation method

To define the collocation method we make use of the same discrete space $\mathcal{U}_h$. The scheme requires a set of collocation points $\{\boldsymbol{\alpha}_A\}_{A=1,\dots,n}$ that are distributed over the domain Ω and sufficiently smooth basis functions. We assume again that the functions $\{N_A\}_{A\in\mathcal{B}}$ are used to impose Dirichlet boundary conditions. We utilize the remaining functions to directly collocate the PDE as

$$\Delta u_h(\boldsymbol{\alpha}_A) + f(\boldsymbol{\alpha}_A) = 0 \quad \text{for all} \quad A \in \mathcal{D} \tag{8}$$

Using the expression of u_h in Eq. (7) and the equations associated to Dirichlet boundary conditions, we obtain a linear system of equations that allows us to compute u_h. The stability and the accuracy of the method depend on the location of the $\boldsymbol{\alpha}_A$'s. Note that the linear systems associated to the collocation and variational method have the same size, but the computation of the matrix and the right hand side vector is significantly faster for collocation methods due to the absence of integrals. However, collocation methods are notably less accurate on a per degree of freedom basis [19].

2.2. The idea of variational collocation

We begin by recalling the *first mean value theorem of integral calculus* [20], which is central to our method.

Theorem 1 (Cauchy, 1821)**.** *Let Ω be a measurable subset of $\mathbb{R}^d$, where d is the number of spatial dimensions. We consider the functions $R : \Omega \mapsto \mathbb{R}$ and $w : \Omega \mapsto \mathbb{R}$. If R is continuous and $w(\boldsymbol{x}) \geq 0$ for all $\boldsymbol{x} \in \Omega$, then, there exists $\boldsymbol{\tau} \in \Omega$ such that*

$$\int_\Omega w(\boldsymbol{x})R(\boldsymbol{x})\mathrm{d}x = R(\boldsymbol{\tau}) \int_\Omega w(\boldsymbol{x})\mathrm{d}x \tag{9}$$

We are now ready to present the idea of variational collocation. Let us first note that the Galerkin form in Eq. (6) is equivalent to

$$\int_\Omega N_A \left(\Delta u_h + f\right) \mathrm{d}x = 0 \quad \text{for all} \quad A \in \mathcal{D} \tag{10}$$

provided that the basis functions $\{N_A\}_{A=1,\dots,n}$ are sufficiently smooth [21]. If we call S_A the support of N_A, that is, the set of points where N_A takes nonzero values, then Eq. (10) is equivalent to

$$\int_{S_A} N_A \left(\Delta u_h + f\right) \mathrm{d}x = 0 \quad \text{for all} \quad A \in \mathcal{D} \tag{11}$$

and assuming that $N_A \geq 0$ on S_A, by Theorem 1, there exists a point $\boldsymbol{\tau}_A \in S_A$ such that

$$0 = \int_{S_A} N_A \left(\Delta u_h + f\right) \mathrm{d}x = \left(\Delta u_h(\boldsymbol{\tau}_A) + f(\boldsymbol{\tau}_A)\right) \int_{S_A} N_A \mathrm{d}x \quad \text{for all} \quad A \in \mathcal{D} \tag{12}$$

which implies that each equation in (6) may be equivalently written as

$$\Delta u_h(\boldsymbol{\tau}_A) + f(\boldsymbol{\tau}_A) = 0 \quad \text{for all} \quad A \in \mathcal{D} \tag{13}$$

for a particular point $\boldsymbol{\tau}_A \in S_A$. Since the support of different basis functions may overlap, it remains to be proven that the points $\{\boldsymbol{\tau}_A\}_{A\in\mathcal{D}}$ are all distinct. We will prove this later for the case in which the N_A's are B-splines, but if we temporarily assume this to hold, it follows that *there exists a set of collocation points that produces exactly the Galerkin solution*. We call the $\boldsymbol{\tau}_A$'s *Cauchy-Galerkin (CG) points*. This is the fundamental idea behind our variational collocation method.

2.3. Scope of variational collocation

Variational collocation only requires the existence of a set of basis functions which are pointwise non-negative, sufficiently smooth and span an appropriate discrete approximation space. In particular, we believe that this idea may have significant impact in some meshless methods [22], maximum-entropy schemes [23] and isogeometric analysis [4, 5], three computational schemes that use basis functions satisfying the necessary conditions for variational collocation. The rest of the paper focuses on isogeometric analysis, but we plan to work on the other topics in the future.

3. Application to isogeometric analysis

A natural application of variational collocation is isogeometric analysis, which is based on the use of splines to construct approximation spaces and define the geometry. IGA has had a significant impact, e.g., in solid mechanics [24, 25, 26, 27, 28, 29], fluid dynamics [10, 30, 31, 32], phase-field modeling [33, 34, 35], contact mechanics [36, 37], biomechanics [38, 39] and fluid-structure interaction [40, 41, 42, 43]. Several types of CAD functions may be used to perform isogeometric analysis, but we will focus on B-Splines and non-uniform rational B-Splines (NURBS), which are pointwise non-negative and can attain $\mathcal{C}^{p-1}$ global continuity for functions of degree p. By restricting our discussion to splines, we will be able to prove the existence of at least n distinct CG points for a space of dimension n. We will also show that the i-th CG point falls within the support of the i-th basis function of the space. Assuming sufficient smoothness, this result holds true independently of the PDE to be solved and shows that it is always possible to find a set of n collocation points which produce the Galerkin solution *exactly*. We begin by reviewing some basic aspects of the theory of B-Splines.

3.1. One-dimensional B-Splines

One-dimensional B-Splines are piecewise polynomials which may be defined as linear combinations of B-Spline basis functions. Let us assume that we work on a parametric space $\mathcal{I}$, which is a closed interval of $\mathbb{R}$. Without loss of generality, we will take $\mathcal{I} = (0, 1)$ in most instances. To define a B-Spline basis, the degree of the engendering polynomial

p and the so-called *knot vector* $\boldsymbol{\Xi}$ need to be specified. The entries of the knot vector $\boldsymbol{\Xi}$, which are called *knots*, are non-decreasing coordinates of the parametric space, such that

$$\boldsymbol{\Xi} = \{\xi_1, \xi_2, \ldots, \xi_{n+p+1}\}. \tag{14}$$

Throughout this paper, we will assume the knot vector to be *open*, that is, $\xi_1 = \ldots = \xi_{p+1}$ and $\xi_{n+1} = \ldots = \xi_{n+p+1}$. This generates a space of dimension n. The zeroth degree B-Spline functions $\{N_{i,(0)}\}_{i=1,\ldots,n}$ are defined as

$$N_{i,(0)}(\xi) = \begin{cases} 1 & \text{if} \quad \xi_i \leq \xi < \xi_{i+1} \\ 0 & \text{otherwise} \end{cases} \quad ; \quad i = 1, \ldots, n. \tag{15}$$

The p-th degree B-Spline basis functions are defined recursively using the relation

$$N_{i,(q)}(\xi) = \frac{\xi - \xi_i}{\xi_{i+p} - \xi_i} N_{i,(q-1)}(\xi) + \frac{\xi_{i+p+1} - \xi}{\xi_{i+p+1} - \xi_{i+1}} N_{i+1,(q-1)}(\xi); \quad i = 1, \ldots, n; \quad q = 1, \ldots, p. \tag{16}$$

The functions $\{N_{i,(p)}\}_{i=1,\ldots,n}$ are $\mathcal{C}^\infty$ everywhere except at the knots. At a non-repeated knot, the functions have $p-1$ continuous derivatives. If a knot has multiplicity m, the number of continuous derivatives at that point is $p-m$. We will call $\mathcal{S}_{p,\boldsymbol{\Xi}}$ the space of splines generated by the functions $\{N_{i,(p)}\}_{i=1,\ldots,n}$. The functions of $\mathcal{S}_{p,\boldsymbol{\Xi}}$ may be pushed forward to a physical space using a geometric mapping and the isoparametric concept. Once we have functions defined on the physical space, they can be utilized to construct discrete approximation spaces, such as $\mathcal{U}_h$ in Sect. 2.1. In turn, these spaces may be employed to discretize equations in variational form. For the sake of simplicity, in the case of one-dimensional problems, we will work on the parametric space, as the role of the geometrical mapping is not so important in this case.

In the rest of the paper, we will omit the subscript indicating the degree in the basis functions of a spline space for the sake of notational simplicity. Therefore, $N_{i,(p)}$ will be simply denoted by N_i and the degree will be inferred from the context.

3.2. Existence of sufficient Cauchy-Galerkin points for isogeometric collocation

In Appendix A we prove that there exist at least n distinct CG points for a spline space of dimension n. Collocation at those points produces the Galerkin solution exactly.

4. Isogeometric collocation at Cauchy-Galerkin points

Within isogeometric analysis, variational collocation may be regarded as isogeometric collocation at CG points (or at their estimates). In this section, we first verify numerically that collocation at the exact CG points reproduces the Galerkin results to machine accuracy, and then proceed to determine estimates of these points to make the method applicable in practice.

4.1. One-dimensional Poisson equation

For simplicity, in this section we focus on a one-dimensional Poisson problem. The goal is to provide numerical evidence that corroborates the theorem proven in Appendix A and show that collocation at CG points produces the Galerkin solution to machine accuracy. Our model problem is defined as

$$u'' + f = 0 \quad \text{in} \quad x \in (0,1) \tag{17}$$

$$u(0) = u(1) = 0 \tag{18}$$

We study the example given by $f(x) = (m_w\pi)^2 \sin(m_w\pi x)$ and $u(x) = \sin(m_w\pi x)$, initially taking $m_w = 1$. Our discrete space is a spline space associated with a uniform, open knot vector on the interval $[0, 1]$, namely,

$$\mathcal{U}^h = \text{span}\{N_i, i = 1, \ldots, n\} \tag{19}$$

The functions N_1 and N_n are used to impose Dirichlet boundary conditions. Therefore, using the notation defined in Sect. 2, we have $\mathcal{B} = \{1, n\}$ and $\mathcal{D} = \{2, \ldots, n-1\}$. We take $p = 3$ and $n = 8$. We compute the Galerkin solution with sufficient quadrature points so as to make the numerical integration error negligible. If we express the Galerkin solution as $u_h = \sum_{B=1}^{n} u_B N_B$ and collect all control variables in the vector $\boldsymbol{U} = \{u_B\}_{B=1,\ldots,n}$ we obtain the solution given by

$$\boldsymbol{U} = \begin{Bmatrix} 0.000000000000000 \\ 0.209433209879956 \\ 0.627801092914975 \\ 1.015982006292745 \\ 1.015982006292745 \\ 0.627801092914974 \\ 0.209433209879956 \\ 0.000000000000000 \end{Bmatrix} \tag{20}$$

Now, we introduce the function $R_h = u_h'' + f$, whose zeros define the CG points; see Eq. (13). Fig. 1 shows a plot of R_h along with the location of Greville points and knots. Greville points are knot averages and are routinely used in isogeometric collocation [11, 13]. It may be observed that, for $p = 3$, CG points are not coincident with Greville points. Indeed, Greville sites seem to be the most distant locations to CG points and coincide with local extrema of R_h, which might explain their poor behavior for cubic splines. Although this model problem is very simple, we observed that this trend prevailed for all the examples we computed with splines of odd degree (see Appendix B).

The CG points may be computed to machine accuracy by finding the roots of the equation $R_h = 0$ using, for example, Newton's method. Let us call $\boldsymbol{g} = \{g_\alpha\}_{\alpha=1,\ldots,n_g}$ the vector of CG points. Due to Theorem 3 in Appendix A, we know that there are at least $n = 8$ CG points, but we ignore *a priori* the precise value of n_g. However, from Fig. 1, we conclude that $n_g = 10$ in this case. Let us call g_α^k the k-th Newton iteration of our iterative

process to find g_α. Then, the problem may be written as: Given a set of initial guesses $\{g_\alpha^0\}_{\alpha=1,\dots,n_g}$, compute

$$g_\alpha^{k+1} = g_\alpha^k - \frac{\sum_{A=1}^n u_A N_A''(g_\alpha^k) + f(g_\alpha^k)}{\sum_{A=1}^n u_A N_A'''(g_\alpha^k) + f'(g_\alpha^k)},\ k = 0, 1, \dots \tag{21}$$

until convergence. We obtain

$$\boldsymbol{g} = \begin{Bmatrix} 0.030539694951151 \\ 0.141211734676611 \\ 0.233391922684160 \\ 0.354128521250408 \\ 0.441699570836731 \\ 0.558300429163268 \\ 0.645871478749592 \\ 0.766608077315842 \\ 0.858788265323387 \\ 0.969460305048849 \end{Bmatrix}. \tag{22}$$

Now, we can utilize the points in Eq. (22) to define our variational collocation method. The problem boils down to defining n collocation points $\boldsymbol{\tau} = \{\tau_A\}_{A=1,\dots,n}$. Since we want to impose Dirichlet boundary conditions strongly on the space, we will take $\tau_1 = 0$ and $\tau_n = 1$, which is equivalent to using the functions N_1 and N_n to enforce the conditions $u_h(0) = u_h(1) = 0$. Therefore, we need to choose $n - 2 = 6$ interior collocation points. Since we have $n_g = 10$ CG points, several choices are possible. In principle, we could choose any subset of $\boldsymbol{g}$ which contains 6 different points with the only restriction that there should be at least one point on the support of each basis function in the space. We have used the sets

$$\boldsymbol{\tau}^1 = \begin{Bmatrix} 0.000000000000000 \\ 0.030539694951151 \\ 0.141211734676611 \\ 0.354128521250408 \\ 0.645871478749592 \\ 0.858788265323387 \\ 0.969460305048849 \\ 1.000000000000000 \end{Bmatrix} \quad \text{and} \quad \boldsymbol{\tau}^2 = \begin{Bmatrix} 0.000000000000000 \\ 0.030539694951151 \\ 0.233391922684160 \\ 0.354128521250408 \\ 0.645871478749592 \\ 0.766608077315842 \\ 0.969460305048849 \\ 1.000000000000000 \end{Bmatrix} \tag{23}$$

In both cases we obtained the control variables defined in (20) to machine accuracy. This result fully supports our theoretical derivations.

4.2. Heuristic study of the location of Cauchy-Galerkin points

Sect. 4.1 shows that collocation at CG points produces the Galerkin solution to machine accuracy. However, it also illustrates that the location of CG points depends on the Galerkin

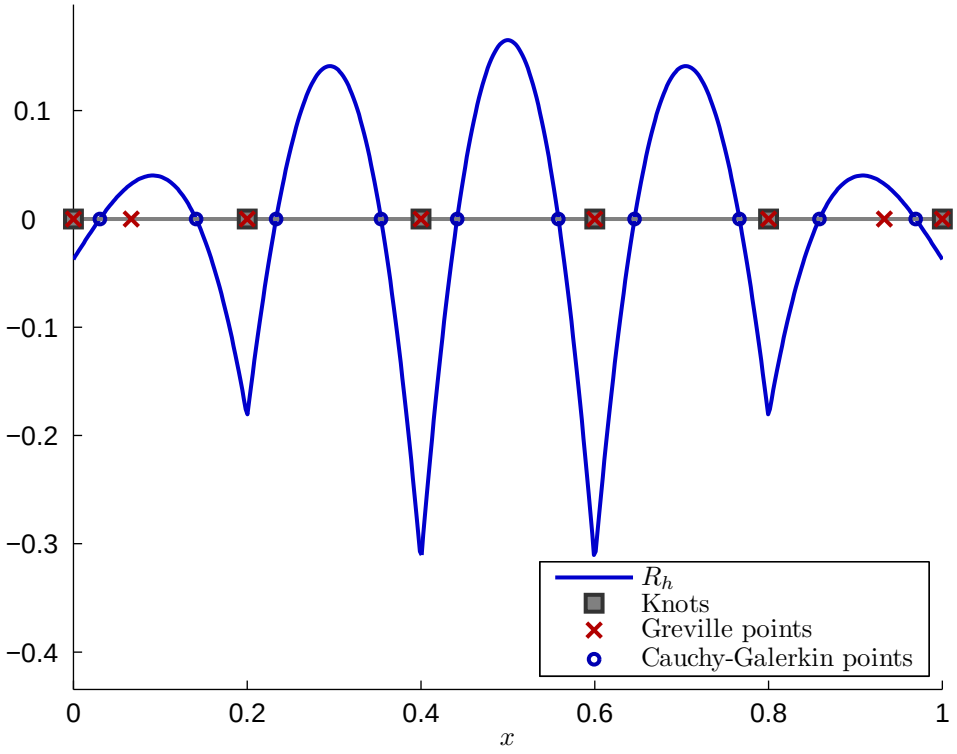

Figure 1: CG points for the one-dimensional Poisson equation. The spline space is defined by $n = 8$, $p = 3$ and an open, uniform knot vector. We use a trigonometric forcing $f(x) = (m_w\pi)^2 \sin(m_w\pi x)$ with $m_w = 1$. The plot shows the function $R_h = u_h'' + f$ as well as the location of CG points, Greville points and knots.

solution itself. This implies that, in order for variational collocation to be practical, an estimate on the location of CG points needs to be provided. For simplicity, in the following we will denote as CG points also their estimates. Before proceeding to derive such an estimate, in this section we summarize the main results of a massive amount of heuristic, exploratory computations performed for splines of maximum continuity.

The first observation emerging from these computations is that the points are strikingly invariant. In particular, their location seems to depend only on the partial differential operator that defines the equation and on the degree of the splines. There is also a very mild dependence on the forcing function f. For example, let us consider again problem (17)–(18). This time, we use a spline space given by $p = 3$, $n = 30$ and a uniform, open knot vector. The forcing function and the exact solution are defined as before, but now we take $m_w = 1$, $m_w = 2$ and $m_w = 3$. The results are shown in Fig. 2. It may be observed that the location of CG points depends very mildly on the forcing function. It is also apparent that CG points follow a simple pattern, essentially with two symmetric occurrences per knot span. The location of the points, relative to the knot span, remains markedly constant. There are approximately twice as many CG points as needed to define a collocation scheme, but we know that any subset will produce the Galerkin solution,

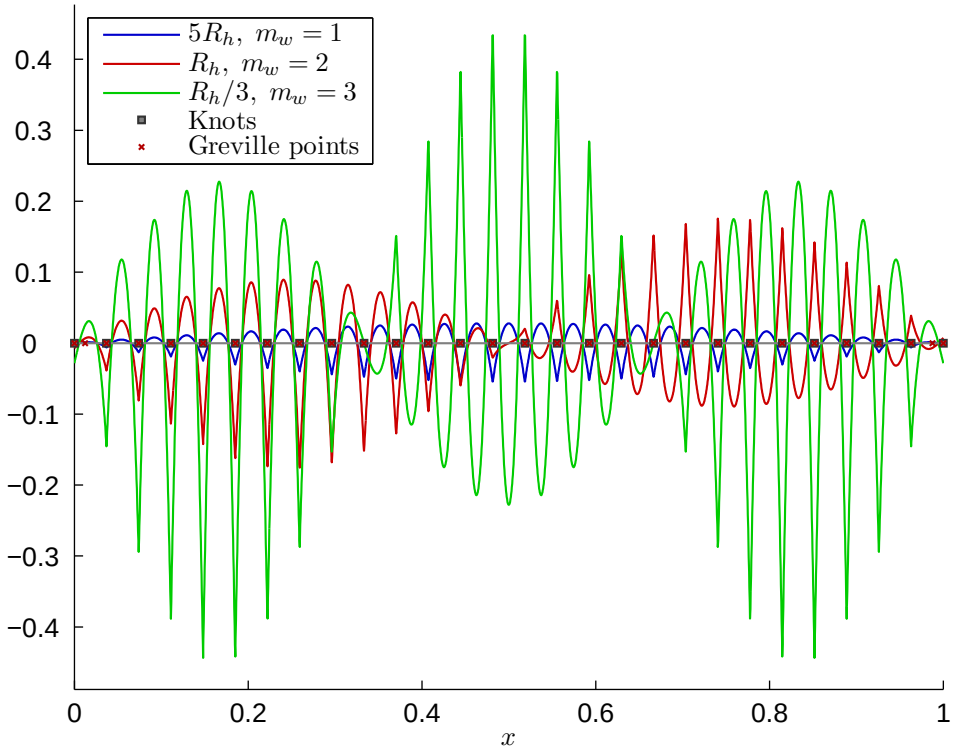

Figure 2: CG points for the one-dimensional Poisson equation. The spline space is defined by $n = 30$, $p = 3$ and an open, uniform knot vector. We use a trigonometric forcing $f(x) = (m_w\pi)^2 \sin(m_w\pi x)$ with $m_w = 1$, $m_w = 2$, $m_w = 3$. The plot shows the function $R_h = u_h'' + f$ as well as the location of CG points, Greville points and knots. With respect to Fig. 1 the function R_h has been rescaled for better visualization of the results.

provided that there is at least one point on the support of each basis function. Again, collocation at Greville points, routinely used thus far, appears to be the worst possible choice. A quantitative study of the location of the points suggests that they fall at the positions $\pm 1/\sqrt{3}$ within a local parameterization $[-1, 1]$ of each knot span.

We studied a number of different cases, varying the degree of the spline space and the forcing function. Some of these examples may be found in Appendix B. All our computations indicate that for $\mathcal{C}^1$-continuous, quadratic splines CG points essentially coincide with Greville points. For splines of maximum continuity and even degree (larger than 2), there are two families of CG points, one located at Greville points and another one at knots. For splines of odd degree, CG points are shifted with respect to Greville sites. These regular patterns apply to the regions of the domain which are sufficiently far from the boundary points or from other "disturbance points" corresponding e.g. to the zeros of the sinusoidal forcing distributions. In the next section, we provide a sound mathematical background to estimate the location of CG points for splines of arbitrary degree.

4.3. Location of Cauchy-Galerkin points based on the superconvergence theory

Thus far, we have defined CG points as the roots of the equation $R_h = u_h'' + f$, where u_h is the Galerkin solution. However, it is trivial to show that $R_h = u_h'' - u''$, which implies that CG points are located where the second derivative of the Galerkin solution is exact. Points at which the first or the second derivative of the Galerkin solution is exact have been widely studied in the context of classical $\mathcal{C}^0$-continuous finite elements [44]. In the realm of linear elasticity, the points at which the derivative of the solution is exact (or at least superconvergent) are referred to as optimal stress points. The points where the second derivative is exact for the bi-Laplace equation and cubic, Hermite basis functions are referred to as Barlow curvature points and have been known for decades [21, 45]. Superconvergent points for the second derivative for the Poisson equation have also been studied in the context of the generalized finite element method [46]. Although the existence and the location of these points have not been widely studied for splines of maximum continuity, it is known that such points exist [47] and they have been recently used for an overdetermined (least-square) collocation scheme [48]. In the following, we present a complete derivation of the location of superconvergent points for splines of maximum continuity.

4.3.1. Splines with $p = 2$ and maximum continuity

For $p = 2$, it is known that superconvergent points for the second derivative are located at the midpoints of each knot span [47]. These points are coincident with Greville points, which confirms that collocation at Greville points for $\mathcal{C}^1$-continuous, quadratic splines and the Laplace operator is a good choice.

4.3.2. Splines with $p = 3$ and maximum continuity

Let us now study the case of $\mathcal{C}^2$-continuous, cubic splines. We consider again problem (17)–(18), with arbitrary forcing, and its Galerkin solution u_h corresponding to a $\mathcal{C}^2$-continuous cubic spline with open knot vector $\boldsymbol{\Xi} = \{\xi_1, \ldots, \xi_{n+p+1}\}$. As before, the discrete space $\mathcal{U}_h$ is spanned by the functions which vanish on the boundary. The remaining functions are used to impose the Dirichlet boundary conditions strongly. We define the error function as $e = u - u_h$. Let us now consider the following one-dimensional Poisson problem

$$v'' + L_i = 0 \quad \text{in} \quad x \in (0, 1) \tag{24}$$

$$v(0) = v(1) = 0 \tag{25}$$

where L_i is a piecewise linear spline, which takes the value 1 at the internal knot ξ_{i+1} and vanishes at ξ_i and ξ_{i+2}. In particular,

$$L_i(x) = \begin{cases} \dfrac{x - \xi_i}{\xi_{i+1} - \xi_i}, & x \in [\xi_i, \xi_{i+1}) \\ \dfrac{\xi_{i+2} - x}{\xi_{i+2} - \xi_{i+1}}, & x \in [\xi_{i+1}, \xi_{i+2}) \\ 0, & \text{otherwise} \end{cases} \tag{26}$$

It may be simply inferred from Eq. (24) that v, i.e., the exact solution to problem (24)–(25) is a $\mathcal{C}^2$-continuous, cubic spline associated to the knot vector $\boldsymbol{\Xi}$, which ensures that $v \in \mathcal{U}_h$. Therefore, we can use v as a weight function in the Galerkin formulation of (24)–(25), which leads to

$$-\int_0^1 v' u_h' \mathrm{d}x + \int_0^1 v L_i \mathrm{d}x = 0 \tag{27}$$

Due to the consistency of the Galerkin formulation, Eq. (27) is also satisfied replacing u_h with u, from which it may be concluded that

$$0 = \int_0^1 v' e' \mathrm{d}x = -\int_0^1 v'' e \mathrm{d}x = \int_0^1 L_i e \mathrm{d}x = \int_{\xi_i}^{\xi_{i+2}} L_i e \mathrm{d}x. \tag{28}$$

Furthermore, on the interior of each knot span, we can Taylor expand e around the midpoint and express the result in terms of Legendre polynomials as

$$e = \begin{cases} c_0^i P_0^i + c_1^i P_1^i + c_2^i P_2^i + c_3^i P_3^i + c_4^i P_4^i + R_i & \text{in } (\xi_i, \xi_{i+1}) \\ c_0^{i+1} P_0^{i+1} + c_1^{i+1} P_1^{i+1} + c_2^{i+1} P_2^{i+1} + c_3^{i+1} P_3^{i+1} + c_4^{i+1} P_4^{i+1} + R_{i+1} & \text{in } (\xi_{i+1}, \xi_{i+2}) \end{cases} \tag{29}$$

where P_m^i denotes the Legendre polynomial of degree m on the interval $[\xi_i, \xi_{i+1}]$, the c_m^i's are the coefficients of the Taylor expansion and $R_i = \mathcal{O}(h^5)$ denotes the remainder. Here, h is a mesh length scale, for example, the knot span length. Our goal is to define a set of equations that allows us to derive the coefficients of the Taylor expansion to eventually find the roots of e'' on each knot span. We note that there are 10 unknown coefficients, but we only need 9 independent equations, because the remaining parameter can be simply thought of as a scaling factor which does not alter the roots of e''. To define these equations, we consider the following:

1. It is known [47] that e' is superconvergent at the knots and the midpoints of the knot span for odd p. In particular, at these points, e' is of order $\mathcal{O}(h^4)$. In the two knot spans that we are considering, this gives us 6 conditions;
2. e is $\mathcal{C}^2$-continuous at ξ_{i+1}, which imposes two constraints on Eq. (29). The first constraint comes from imposing that e is continuous at ξ_{i+1} and the second one from enforcing the continuity of e'' at ξ_{i+1}. Imposing the continuity of e' at ξ_{i+1} would produce an equation that is linearly dependent on the constraints that ensure superconvergence of e' at knots;
3. e satisfies Eq. (28).

This produces 9 independent equations which lead to the result

$$c_0^i = c_0^{i+1} = c_1^i = c_1^{i+1} = c_3^i = c_3^{i+1} = \mathcal{O}(h^5), \tag{30}$$

$$c_4^i - c_4^{i+1} = \mathcal{O}(h^5), \tag{31}$$

$$c_4^i + \frac{3}{10} c_2^i = \mathcal{O}(h^5). \tag{32}$$

From Eqns. (29) and (30)–(32), we obtain

$$e = c_2^i \left(P_2^i - \frac{3}{10} P_4^i \right) + \mathcal{O}(h^4) \quad \text{in} \quad [\xi_i, \xi_{i+1}] \tag{33}$$

Eq. (33) can be mapped to the interval $[-1, 1]$ to standardize the location of CG points. If we call e_R the error function on the interval $[-1, 1]$, rescaled to eliminate the missing constant c_2^i, we conclude that, to leading order,

$$e_R(\eta) \approx P_2(\eta) - \frac{3}{10} P_4(\eta) \quad \eta \in [-1, 1] \tag{34}$$

where P_2 and P_4 are, respectively, the quadratic and quartic Legendre polynomials in the interval $[-1, 1]$, i.e.,

$$P_2 = \frac{1}{2}(3\eta^2 - 1) \tag{35}$$

$$P_4 = \frac{1}{8}(35\eta^4 - 30\eta^2 + 3) \tag{36}$$

Direct differentiation of Eq. (34) leads to $e_R''(\eta) \approx 21(1 - 3\eta^2)/4$, which indicates that CG points for the Laplace equation and $\mathcal{C}^2$-continuous, cubic splines are located at

$$\eta = \pm 1/\sqrt{3}, \tag{37}$$

which is consistent with the numerical results presented in Sect. 4.2 and Appendix B.

4.3.3. Splines with arbitrary p and maximum continuity

A general procedure to derive the error function and thus the location of the CG points for the Laplace equation is reported in Appendix C. A summary of the error functions and of the location of the CG points is provided in Tabs. C.2 and C.3, respectively.

4.4. Generalization to different equations, multiple dimensions and non-linear problems

Thus far, we have focused on the Poisson problem. This section shows how the idea of variational collocation may be extended to many other problems of interest in computational mechanics. For example, let us consider the problem

$$u^{(4)} + f = 0 \tag{38}$$

with appropriate boundary conditions. Eq. (38) may be thought of as a Poisson problem for u''. If we call u_h the Galerkin solution to Eq. (38) using a spline space of degree p and maximum continuity, then it is clear that u_h'' belongs to a spline space of degree $p-2$ whose basis functions are $\mathcal{C}^{p-3}$-continuous where u_h is $\mathcal{C}^{p-1}$-continuous. Therefore, it follows that the CG points associated to Eq. (38) are given by the roots of the second derivative of the error function for splines of degree $p - 2$. For example, if we solve Eq. (38) using splines of degree $p = 5$, CG points are located exactly as indicated in Eq. (37), i.e., at the roots

of the second derivative of the error function for cubic splines. In the section devoted to numerical examples, we exploit this idea to apply variational collocation to the analysis of Kirchhoff plates.

Let us give another example of how our ideas may be extended to more general situations. It may be shown [47] that all the results presented in Sect. 4.3 hold true replacing the model problem (17)–(18) by the more general boundary value problem

$$-(\kappa(x)u')' - (a(x)u)' + r(x)u = f \quad \text{in} \quad (0,1) \tag{39}$$

$$u(0) = u(1) = 0 \tag{40}$$

where $\kappa : (0,1) \mapsto \mathbb{R}^+$, $a : (0,1) \mapsto \mathbb{R}$ and $r : (0,1) \mapsto \mathbb{R}$. This opens the possibility of solving advection-diffusion-reaction problems using variational collocation.

Reference [47] also shows that the results proven in Sect. 4.3 can be trivially extended to tensor product spaces. In this case, the superconvergent points are determined by computing the tensor product of the coordinates of the one-dimensional points. This is a case of obvious interest for isogeometric analysis, because the most widely utilized type of functions, namely, NURBS, in the multivariate case are generated as the weighted tensor product of their univariate counterparts and retain all the important properties of tensor products. The extension to multivariate cases might be less obvious for other basis functions. For example, in the last few years T-splines have emerged as a promising alternative to NURBS for IGA [13, 49, 16, 50]. T-splines are tensor products of splines locally, but not globally. Therefore, the location of CG points for these functions is not obvious *a priori* but would be a very promising research line.

The above remarks imply that, for discrete spaces of NURBS, all the derivations in Sect. 4.3 are valid for a multidimensional domain $\Omega \subset \mathbb{R}^d$, with $d = 2$ or $d = 3$ and for the problem

$$-\nabla \cdot (\boldsymbol{\kappa}(\boldsymbol{x})\nabla u) - \nabla \cdot (\boldsymbol{a}(\boldsymbol{x})u) + r(\boldsymbol{x})u = f \quad \text{in} \quad \Omega \tag{41}$$

$$u = u_D \quad \text{on} \quad \Gamma \tag{42}$$

where Γ is the boundary of Ω and u_D is a known function. To solve problem (41)–(42), the usual approach is to map the spline space from a parametric domain to Ω. The question of whether CG points in Ω are simply the transformation of their parametric analogue using the geometric map arises naturally. Reference [47] shows that this is indeed the case for isoparametric mappings.

Finally, it may be shown [47] that, under certain assumptions, superconvergent points for a non-linear problem coincide with those associated to its linearization.

Collectively, these considerations suggest that variational collocation may find application in numerous areas of computational mechanics, including, e.g., linear and non-linear elasticity, advection-diffusion-reaction problems[2], thin plates and shells and phase-field

[2]For advection-dominated problems, a study of the location of CG points for stabilized formulations would be necessary.

modeling. The numerical examples in Sect. 5 fully support this conclusion. In particular, they demonstrate that, for linear and non-linear elasticity problems in two and three dimensions as well as for Kirchhoff plates, variational collocation, i.e., isogeometric collocation at Cauchy-Galerkin points, clearly outperforms standard isogeometric collocation. In particular, the former achieves a spatial convergence order (in the $\mathcal{L}^2$ and $\mathcal{H}^1$ norms of the displacement error) of p for any order of discretization, thus increasing by one the known convergence order for splines of odd degree.

Note that, despite this significant improvement, the rate of p is still lower by one than the analogous rate which would be achieved with the Galerkin method. The reason is the fact that, as noted earlier, CG points can only be *estimated*, as their exact computation (at least at the current state of knowledge) would require the prior solution of the Galerkin problem. Moreover, the estimate based on superconvergence is limited to the interior of the domain, far from the "disturbance points" mentioned in Sect. 4.2. Improvements in the estimate should lead to corresponding improvements in the convergence rate and may be considered in further research.

5. Numerical examples

This section presents two- and three-dimensional examples which demonstrate the accuracy of variational collocation in the isogeometric context, i.e., of isogeometric collocation at CG points as opposed to standard isogeometric collocation at Greville points (the use of Demko points is known to yield nearly identical results to collocation at Greville points). We focus on linear and non-linear elasticity and we also address Kirchhoff plates. For splines of even degree, as Greville points are a subset of CG points, we simply use Greville points, whereas for splines of odd degrees we use the CG points given in Tab. C.3. For simplicity, when we use odd degree interpolations we adopt an odd number of knot spans in each parametric direction.

5.1. Linear and nonlinear elasticity

We begin by describing how we compute CG points for splines of odd degree in the case of second-order PDE's. The dimension of the spline space is lower than the total number of CG points. As shown before, if the exact location of the CG points is used any subset that hits every function in the space will produce the Galerkin solution exactly. If the location of CG points is only approximate, there might be some sensitivity to the subset taken, although we did not observe that. Therefore, we simply took a subset with a symmetric spatial distribution that uses one point per knot span away from the boundary and the central knot span. In Listing 1, we provide a MATLAB® code that produces the CG points that we have used in our computations.

Listing 1: Matlab code to compute Cauchy-Galerkin points for second-order PDEs

```
% DATA: Polynomial degree: p              [Assumed to be 3, 5 or 7]
% DATA: Number of control points: ncp     [Assumed to be even]
% RESULTS: Cauchy-Galerkin points: cg(:) [The length of cg is ncp]
```

```
% REQUIREMENTS: Spline Toolbox
function [cg]=CauchyGalerkin(p,ncp)
nspn = ncp - p;                    % Compute the number of knot spans
knot = augknt(0:1/nspn:1,p+1);     % Compute a uniform knot vector
ksle = knot(p+2) - knot(p+1);      % Compute the knot span length
grev = aveknt(knot,p+1);           % Compute Greville points
% Normalized CG point (Tab. C.3)
if (p==3); ncgp = 1/sqrt(3);                    end
if (p==5); ncgp = sqrt(225-30*sqrt(30))/15;     end
if (p==7); ncgp = 0.5049185675126533;           end
ofst = ksle*(1-ncgp)/2;            % Compute offset wrt Greville
% Compute CG points from Greville points
cg(1:ncp/2)      = grev(1:ncp/2)      + ofst;
cg(ncp/2+1:ncp) = grev(ncp/2+1:ncp) - ofst;
cg(1)            = 0;              % We assume Dirichlet BC at x=0
cg(ncp)          = 1;              % We assume Dirichlet BC at x=1
```

5.1.1. Linear elasticity: Dirichlet problem with manufactured solution

The first example is a quarter of annulus (Fig. 3) with $R_i = 1$ and $R_o = 4$, clamped at the entire boundary, made of a linearly elastic material with Lamé constants $\lambda = \mu = 1$. The displacement field is denoted $\boldsymbol{u} = \{u, v\}$. The domain is subjected to a body force which is computed so as to satisfy the prescribed boundary conditions and to correspond to the following manufactured solution:

$$\begin{cases} u_{ref} &= xy(x^2 + y^2 - 1)(x^2 + y^2 - 16) \\ v_{ref} &= u_{ref} \end{cases} \tag{43}$$

which then serves as reference solution $\boldsymbol{u}_{ref}$ for the convergence study. Results in terms of the $\mathcal{L}^2$ norm and the $\mathcal{H}^1$ seminorm of the error are illustrated in Fig 4. It is evident that, while results obtained from both sets of collocation points for even interpolation degrees are obviously identical and feature for both norms a convergence rate of p, odd interpolation degrees lead to a convergence rate of $p-1$ for collocation at Greville abscissae and of p for the CG points. In other words, collocation at CG points guarantees for both considered norms a convergence rate of p for all values of p, regardless whether even or odd.

5.1.2. Linear elasticity: infinitely long cylinder under inner pressure

As a second benchmark, we consider an infinitely long cylinder subjected to uniform internal pressure. The problem can be solved in 2D adopting plane strain assumptions, and we further exploit symmetry considering only a quarter of annulus, see Fig. 5. We adopt $R_i = 1$ and $R_o = 4$, an inner pressure $\bar{p} = 0.5$, and consider a linearly elastic material with Lamé constants $\lambda = \mu = 1$. The exact solution is given by

$$u_{r,ref} = \frac{\bar{p}\,(1+\nu)}{E} \frac{R_i^2}{R_o^2 - R_i^2} \left[(1-2\nu)\, r + \frac{R_o^2}{r} \right] \tag{44}$$

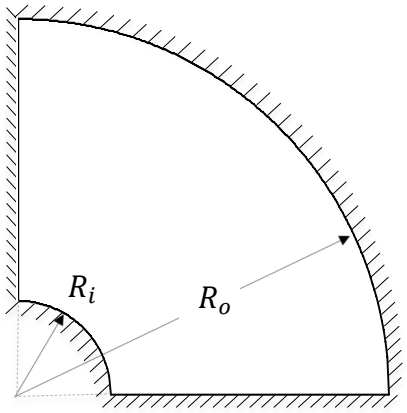

Figure 3: Linear elasticity: Dirichlet problem with manufactured solution. Geometry and boundary conditions.

where u_r is the radial displacement, r is the radial coordinate (ranging between R_i and R_o), and E and ν are respectively the elastic modulus and Poisson's ratio of the material, which can be derived from λ and μ using well-known relationships. Note that, due to the axisymmetric nature of the problem, the circumferential displacement u_θ is identically zero in the entire domain.

Fig. 6 reports the convergence study for this case. Results confirm those observed in the previous example, with collocation at Greville points featuring a convergence rate of $p-1$ and p for odd and even degrees, respectively, and collocation at CG points leading to a convergence rate of p for all degrees for both considered norms.

5.1.3. Nonlinear hyperelasticity: infinitely thick cylinder under inner pressure

In this example, we aim at demonstrating the advantages of using CG points for collocation also in non-linear problems. In particular, we adopt a kinematically non-linear framework and assume for the material the neo-Hookean constitutive law proposed in [51]. The corresponding strain energy density is

$$\psi = \frac{\mu}{2}\left(I_C - 3\right) - \mu \ln J + \frac{\lambda}{2}\left(\ln J\right)^2 \tag{45}$$

where I_C is the first invariant of the right Cauchy-Green deformation tensor, and J is the determinant of the deformation gradient. For details about isogeometric collocation in hyperelasticity see [18].

Geometry, loading condition and Lamé constants are the same as in Section 5.1.2. As no analytical solution is available in this case, we use as reference for the convergence study an overkill solution obtained from a mesh with 400 control points in each parametric direction. Results are shown in Fig. 7. It is evident that the convergence properties of collocation at CG points already obtained from the examples in linear elasticity are further confirmed

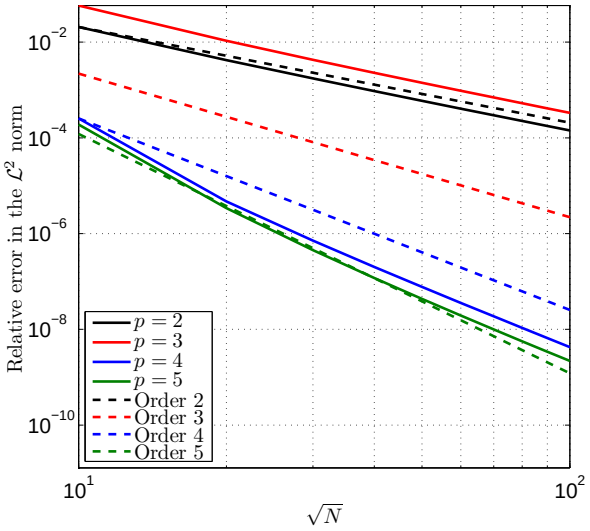

(a) Greville points, $\mathcal{L}^2$ norm

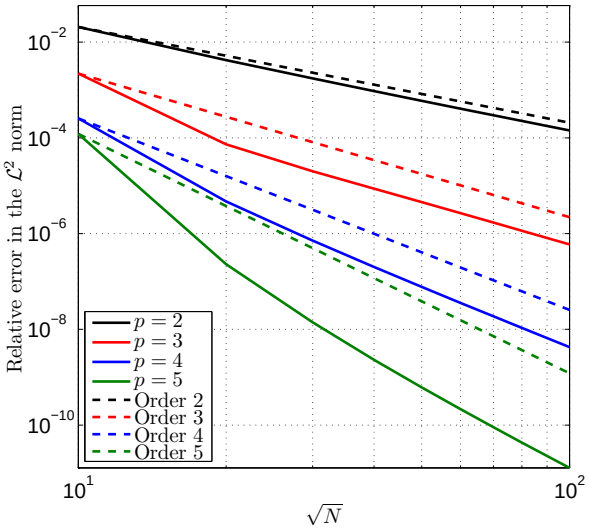

(b) CG points, $\mathcal{L}^2$ norm

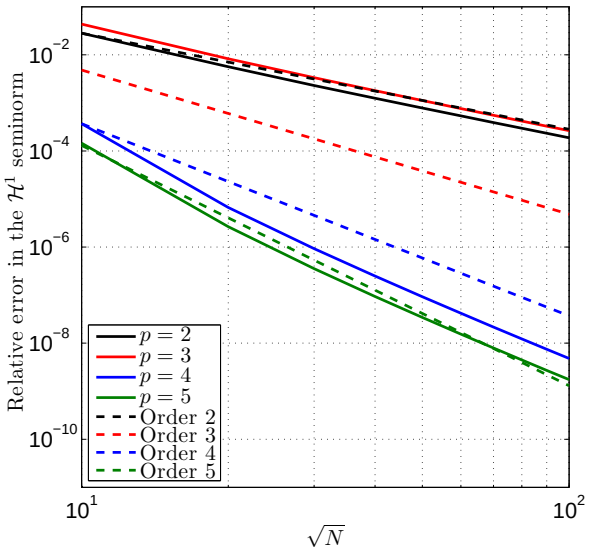

(c) Greville points, $\mathcal{H}^1$ seminorm

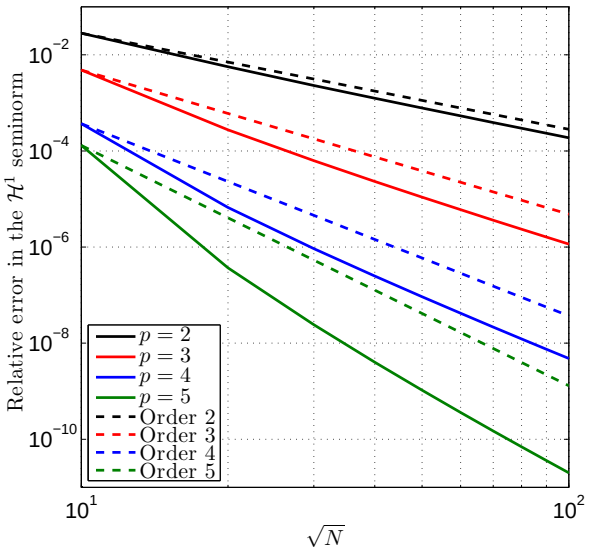

(d) CG points, $\mathcal{H}^1$ seminorm

Figure 4: Convergence rates in the $\mathcal{L}^2$ norm (top row) and the $\mathcal{H}^1$ seminorm (bottom row) for the Dirichlet problem with manufactured solution in linear elasticity. N denotes the total number of degrees of freedom. For odd degrees, collocation at CG points produces significantly smaller errors than collocation at Greville points and increases the rate of convergence by one.

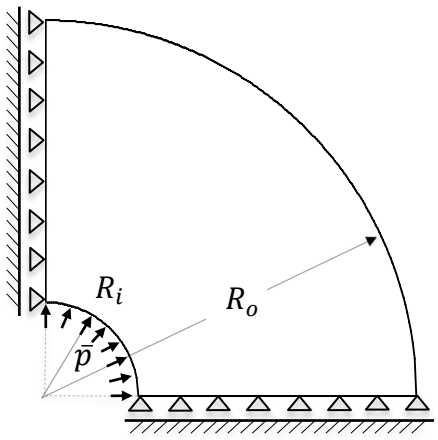

Figure 5: Linear elasticity: infinitely thick cylinder under inner pressure. Geometry and boundary conditions.

in the hyperelastic framework. Once again collocation at these points achieves the same convergence rate of p, regardless whether p is even or odd, for both considered norms.

5.1.4. Nonlinear hyperelasticity: hollow sphere under inner pressure

We demonstrate here the extension of the approach to the three-dimensional setting. We consider a thick hollow sphere with inner radius $R_i = 1$ and outer radius $R_o = 2$, subjected to a uniform outward radial displacement on the inner surface $\bar{u}_r = 0.2$. Due to symmetry we only model one eighth of the geometry (Fig. 8) with symmetric boundary conditions. We adopt again a kinematically non-linear framework with the neo-Hookean constitutive law already used in Sect. 5.1.3. We limit ourselves to the case $p = 3$ and compare Galerkin results with those obtained with collocation at Greville and at CG points for two different meshes, denoted in Tab. 1 by the number of control points in the three parametric directions. The relative error is computed as

$$e_{\mathcal{L}^2} = \frac{\|u_r - u_{r,Gal}\|_2}{\|u_{r,Gal}\|_2} \tag{46}$$

where u_r is the radial displacement field computed with collocation, $u_{r,Gal}$ is the same field obtained from the standard Galerkin approach, and $\|\cdot\|_2$ is the $\mathcal{L}^2$ norm. Once again it is evident that, for $p = 3$, results from collocation at CG points are significantly closer to Galerkin results than those from collocation at Greville points.

5.2. Kirchhoff plates

The theory presented in Sect. 4.3 permits obtaining an estimate of CG points also for fourth-order operators, which is an area of computational mechanics where methods based on smooth basis functions shine. To illustrate the performance of our method in this

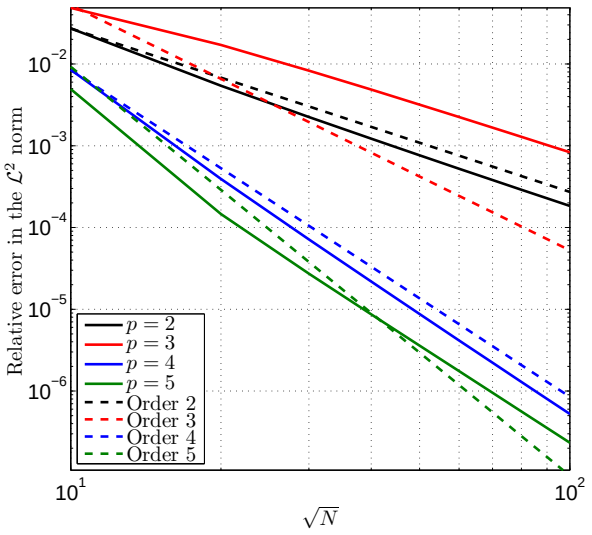

(a) Greville points, $\mathcal{L}^2$ norm

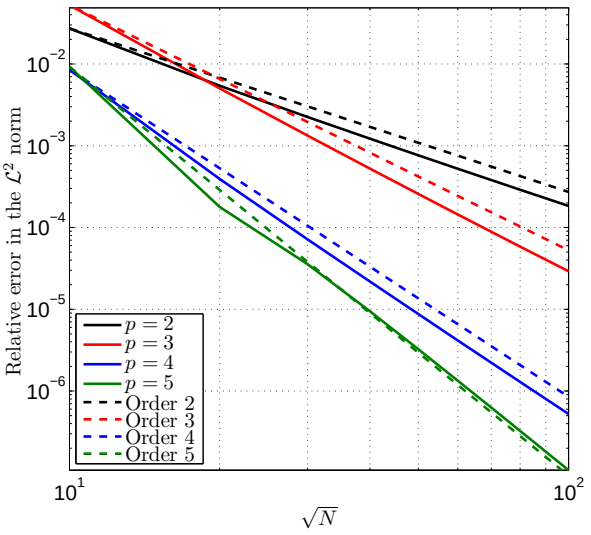

(b) CG points, $\mathcal{L}^2$ norm

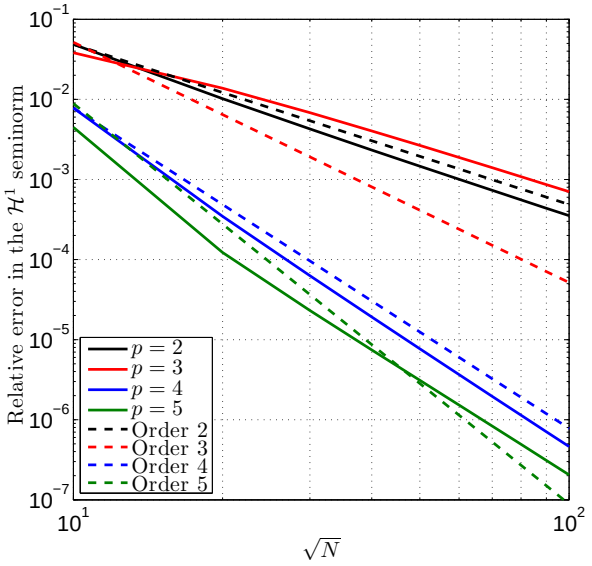

(c) Greville points, $\mathcal{H}^1$ seminorm

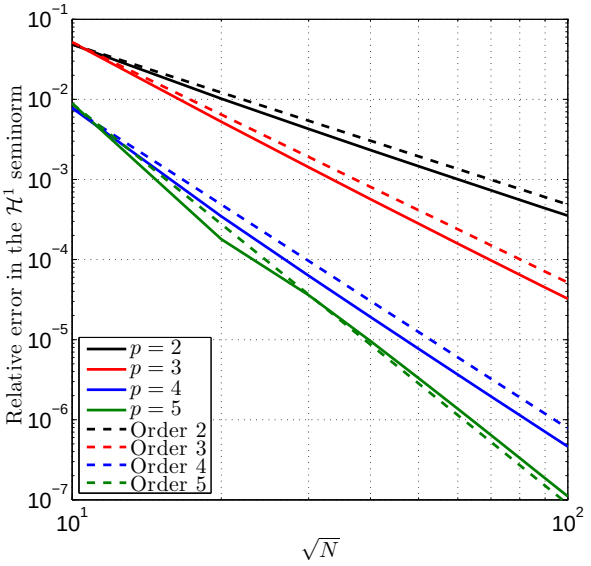

(d) CG points, $\mathcal{H}^1$ seminorm

Figure 6: Convergence rates in the $\mathcal{L}^2$ norm (top row) and the $\mathcal{H}^1$ seminorm (bottom row) for the infinitely long cylinder under inner pressure in linear elasticity. N denotes the total number of degrees of freedom. For odd degrees, collocation at CG points produces significantly smaller errors than collocation at Greville points and increases the rate of convergence by one.

	Greville	CG
Mesh 1: 10×20×6	0.0109	0.00327
Mesh 2: 20×40×12	0.00197	0.000120

Table 1: Relative error with respect to the Galerkin solution for the hollow sphere under inner pressure in hyperelasticity.

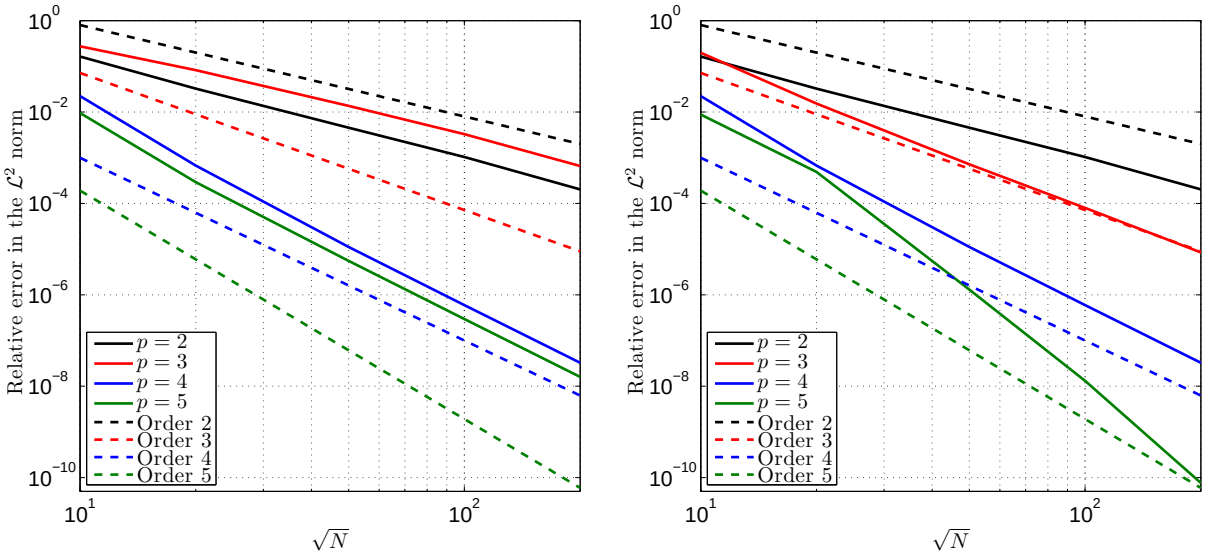

(a) Greville points, $\mathcal{L}^2$ norm

(b) CG points, $\mathcal{L}^2$ norm

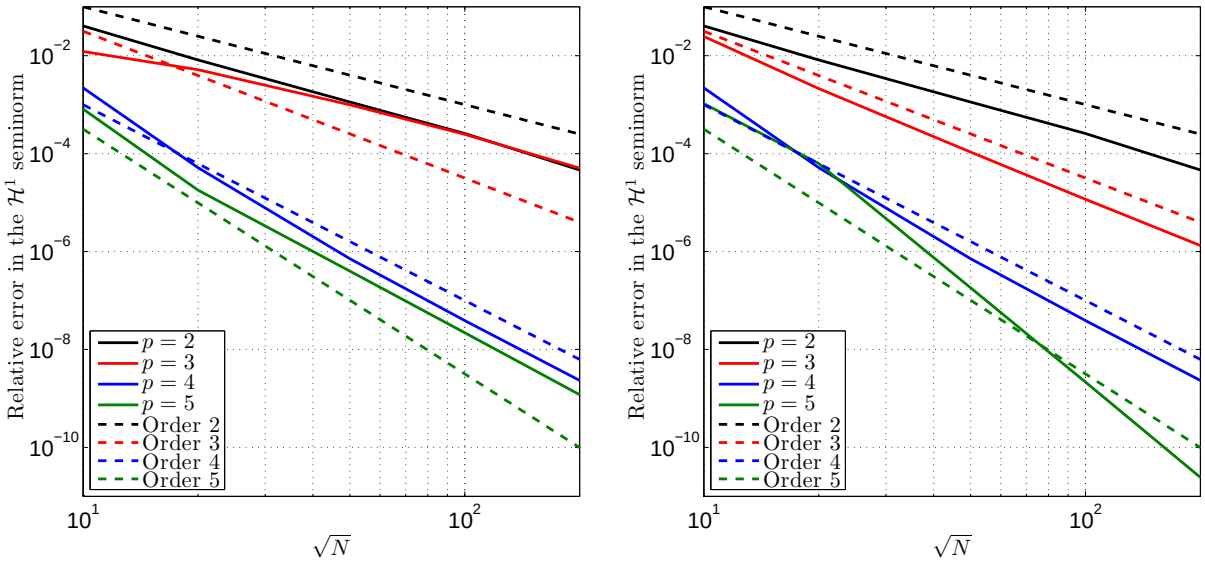

(c) Greville points, $\mathcal{H}^1$ seminorm

(d) CG points, $\mathcal{H}^1$ seminorm

Figure 7: Convergence rates in the $\mathcal{L}^2$ norm (top row) and the $\mathcal{H}^1$ seminorm (bottom row) for the infinitely thick cylinder under inner pressure in hyperelasticity. N denotes the total number of degrees of freedom. For odd degrees, collocation at CG points produces significantly smaller errors than collocation at Greville points and increases the rate of convergence by one.

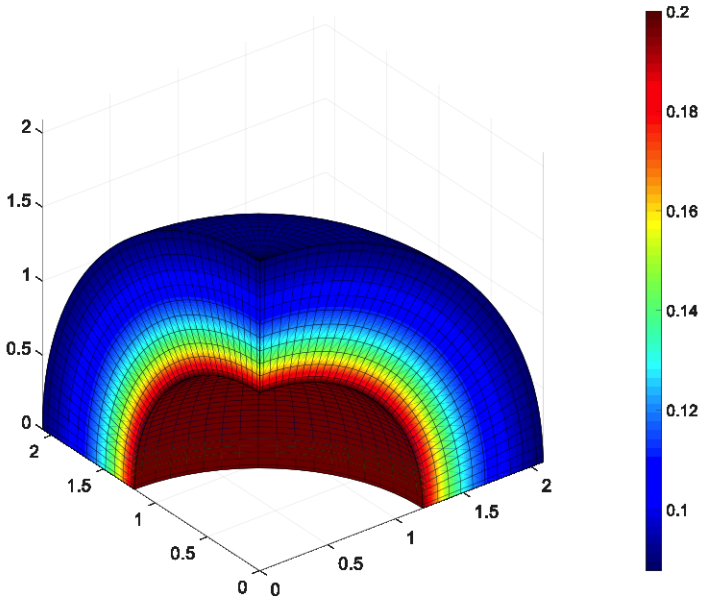

Figure 8: Hyperelasticity: hollow sphere under inner pressure. Geometry and contour plot of the radial displacements.

situation, we solve a simple benchmark problem involving Kirchhoff plates. We consider a clamped plate over the domain $\Omega = [0, 1]^2$. The problem is defined by

$$D\Delta^2 w = q \quad \text{in} \quad \Omega \tag{47}$$

$$w = 0 \quad \text{on} \quad \Gamma \tag{48}$$

$$\nabla w \cdot \boldsymbol{n} = 0 \quad \text{on} \quad \Gamma \tag{49}$$

where Δ^2 represents the bi-Laplace operator, Γ is the boundary of Ω and D is a constant that depends on the material properties and the thickness of the plate. In our computations, we take $D = 1$ and

$$q(x, y) = -16\pi^4[\cos(2\pi x) - 4\cos(2\pi x)\cos(2\pi y) + \cos(2\pi y)], \tag{50}$$

which leads to the exact solution

$$w(x, y) = [1 - \cos(2\pi x)][1 - \cos(2\pi y)] \tag{51}$$

To define the discrete space, we utilize splines constructed as the tensor product of a uniform one-dimensional space with n control variables. Therefore, the two-dimensional space has n^2 control variables associated. Our collocation strategy is as follows: For even p, CG points essentially coincide with Greville points, so we proceed as in [52]. For odd p, CG points are shifted with respect to Greville sites (their location may be found in Tab.

C.3), which suggests that new collocation sites should be adopted. Due to the continuity requirements imposed by the governing equation, the lowest odd degree that may be utilized is $p = 5$, which produces $\mathcal{C}^4$-continuous splines when the interior knots are not repeated. We present results for the odd degrees $p = 5$ and $p = 7$, but the ideas can be easily extended to arbitrarily high degrees. According to the discussion in Sect. 4.4 and the results in Tab. C.3, CG points are located at $\eta = \pm 1/\sqrt{3}$ for $p = 5$ and $\eta = \pm\sqrt{225 - 30\sqrt{30}}/15$ for $p = 7$. We impose the condition (48) strongly on the space, which constrains the control variables falling on the topological boundary of the mesh. Eq. (49) is collocated at the border, skipping the corner points and averaging some equations, exactly as explained in [52]. After this, we still need to impose $(n-4)^2$ equations to define a square linear system. Due to the tensor product structure of our spline space, we just need to define $n - 4$ interior collocation points in one parametric direction, compute their tensor product and use them to collocate Eq. (47). Once the location of these $n-4$ points is given, our method is completely defined. For odd-degree splines, the location of these points varies slightly with p. We define the points for $p = 5$ and $p = 7$. The extension to higher degrees is straightforward. For simplicity, let us consider a case with an odd number of knot spans. In such case, we can define a central knot span. The remaining knot spans are classified as being on the left or the right hand side of the central. It is known that there are two CG points on each knot span. For $p = 5$, we use two CG points on the central knot span. For the remaining knot spans we use just one CG point, which completes the $n - 4$ points needed. For the knot spans on the left (right) of the central span, we employ the leftmost (rightmost) CG point. For $p = 7$ the collocation points are analogous, but we also use two CG points in the first and the last knot spans. Fig. 9 shows the location of the points for $p = 5$ and $p = 7$.

We used the approach described above to solve Eqns. (47)–(50) and computed the $\mathcal{L}^2$ norm of the deflection, rotation, bending moment and shear force error using the expression of the exact solution given in (51). For comparison purposes, we report also the results using classical collocation at Greville points; see Fig. 10(a)-(c) and Fig. 11(a)-(c). The results using our approach are shown in Fig. 10(b)-(d) and Fig. 11(b)-(d). As expected, the results for even p are identical. However, for odd p our method clearly outperforms collocation at Greville points. The convergence rate for splines of odd degree is $p-3$ using collocation at Greville sites and $p - 2$ using collocation at CG points. The results are consistent with those obtained for linear and non-linear elasticity.

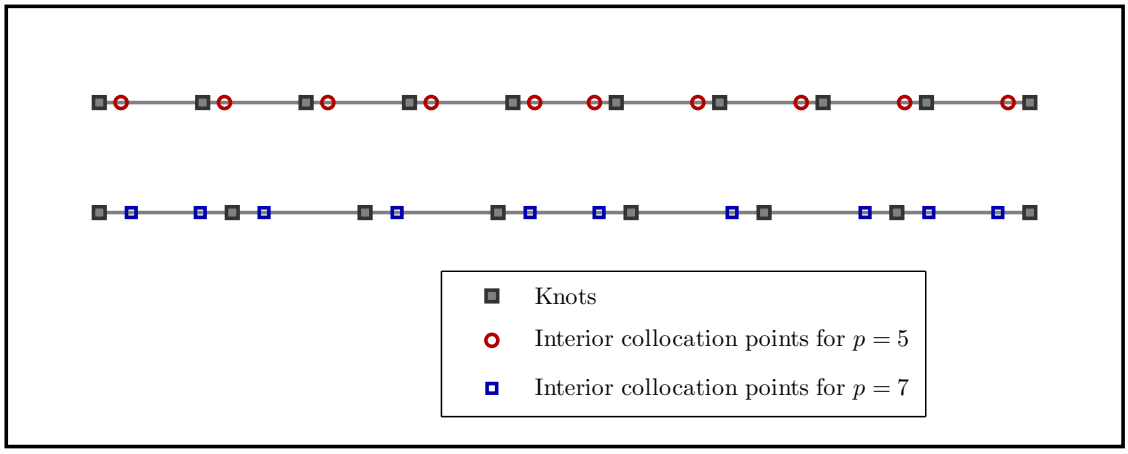

Figure 9: Example of the interior collocation points for $p = 5$ (top) and $p = 7$ (bottom) in the case of Kirchhoff plates. The actual collocation points are defined by taking the tensor product of each of the one-dimensional cases with themselves. For $p = 5$ we use two collocation points in the central span. For $p = 7$ we use two collocation points in the central, the first and the last knot spans.

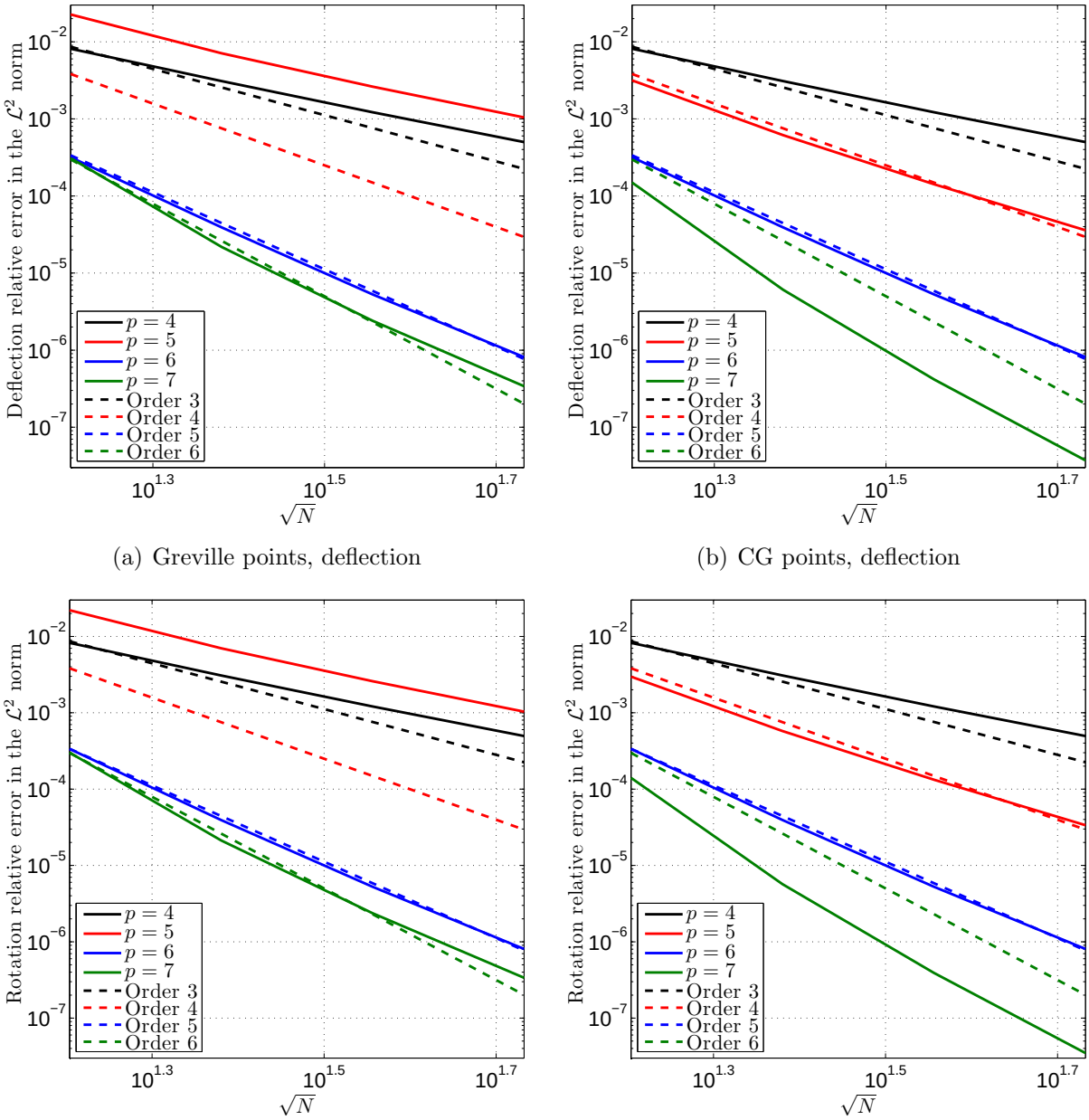

(a) Greville points, deflection

(b) CG points, deflection

(c) Greville points, rotation

(d) CG points, rotation

Figure 10: Convergence rates in the $\mathcal{L}^2$ for a clamped Kirchhoff plate with a manufactured load. The top row shows deflections and the bottom row rotations. N denotes the total number of degrees of freedom. For odd degrees, collocation at CG points produces significantly smaller errors than collocation at Greville points and increases the rate of convergence by one.

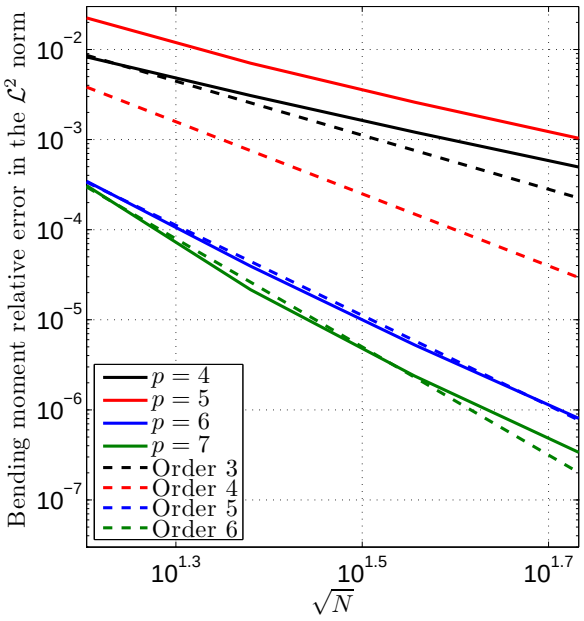

(a) Greville points, bending moment

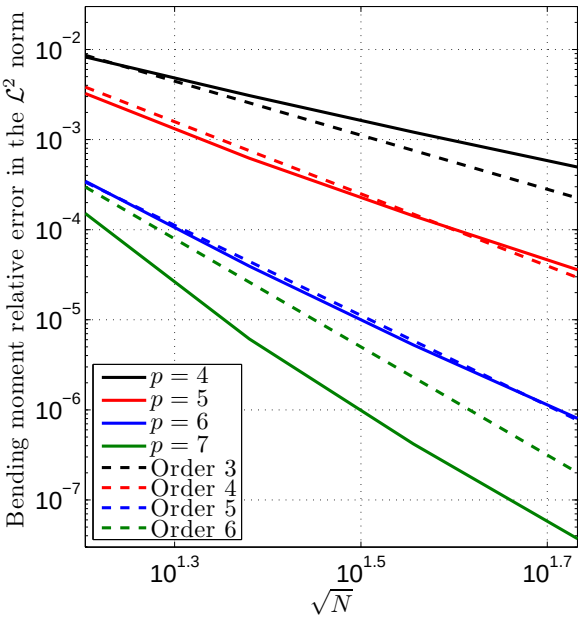

(b) CG points, bending moment

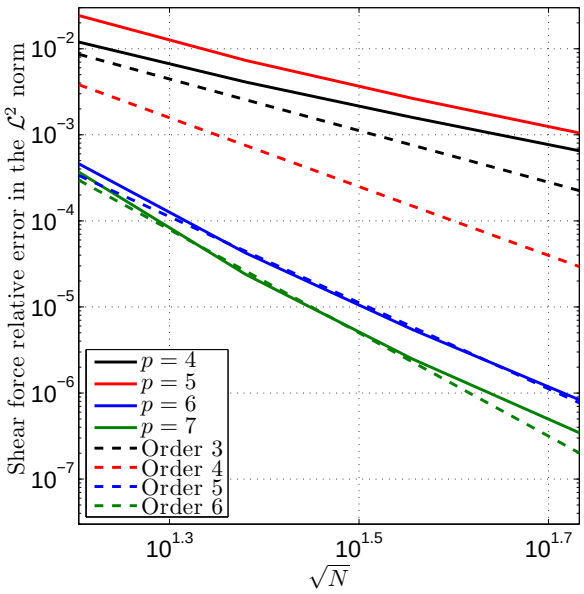

(c) Greville points, shear force

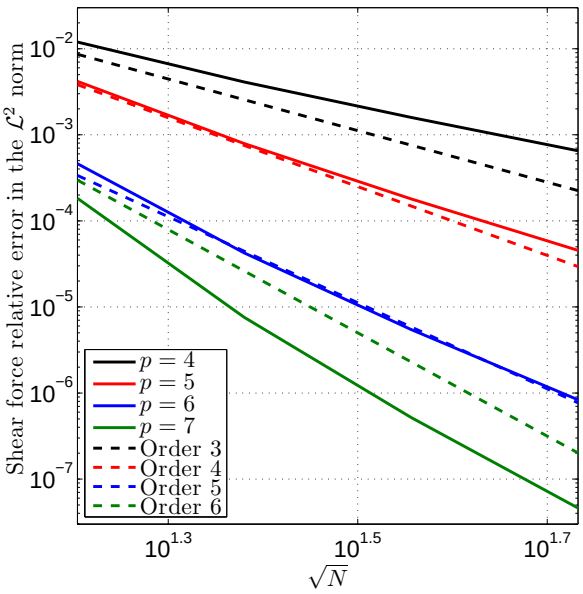

(d) CG points, shear force

Figure 11: Convergence rates in the $\mathcal{L}^2$ for a clamped Kirchhoff plate with a manufactured load. The top row shows bending moments and the bottom row shear forces. N denotes the total number of degrees of freedom. For odd degrees, collocation at CG points produces significantly smaller errors than collocation at Greville points and increases the rate of convergence by one.

6. Opportunities: reduced quadrature schemes for isogeometric analysis

We believe that the concept of variational collocation may open a number of new possibilities in computational mechanics. As target areas, we envision in particular the problems in which standard collocation has proven to be insufficiently accurate or robust with respect to Galerkin methods. These include some non-linear (in particular non-smooth) problems or problems prone to locking. Moreover, we believe that variational collocation could also lead to the development of new reduced quadrature schemes. As follows, we provide an exploratory example of the latter application.

Let us consider a linear elasticity problem in the weak form. The problem domain is $\Omega \subset \mathbb{R}^d$. For simplicity, we consider zero-displacement boundary conditions in all directions on the entire boundary. Letting $\mathcal{U}_h$ denote a suitable discrete space, the problem may be written in Galerkin form as: Given the vector of body forces $\boldsymbol{f} : \Omega \mapsto \mathbb{R}^d$, find the displacement field $\boldsymbol{u}_h \in \mathcal{U}_h$ such that

$$\int_\Omega \nabla \boldsymbol{w}_h : \boldsymbol{\sigma} \, \mathrm{d}x = \int_\Omega \boldsymbol{w}_h \cdot \boldsymbol{f} \mathrm{d}x \quad \text{for all} \quad \boldsymbol{w}_h \in \mathcal{U}_h, \tag{52}$$

where $\boldsymbol{\sigma}$ is the Cauchy stress tensor. If we define $\mathcal{U}_h$ using a spline space of degree p in all directions, and assuming that there is no geometrical mapping, the exact evaluation of the stiffness matrix using element-based Gaussian quadrature requires $(p+1)^d$ evaluation points per element[3]. Integration formulas which do not integrate exactly all the polynomials in the bilinear form given an affine mapping are called reduced quadratures.

For sufficiently smooth basis functions, and sufficiently accurate numerical integration, Eq. (52) is equivalent to

$$\int_\Omega \boldsymbol{w}_h \cdot \nabla \cdot \boldsymbol{\sigma} \, \mathrm{d}x + \int_\Omega \boldsymbol{w}_h \cdot \boldsymbol{f} \, \mathrm{d}x \quad \text{for all} \quad \boldsymbol{w}_h \in \mathcal{U}_h, \tag{53}$$

Under the same conditions as before, i.e., $\mathcal{U}_h$ is a spline space of degree p in all directions defined in the parametric domain, the exact evaluation of the first integral in Eq. (53) using element-based Gaussian integration also requires $(p+1)^d$ quadrature points per element.

Reduced quadrature rules have been extensively investigated in the field of finite elements and, in particular, in isogeometric methods [53, 54]. However, as far as we are aware, these studies focus on the weak form given in Eq. (52).

We believe that variational collocation opens new opportunities to derive reduced quadrature formulas for the weighted residual formulation of the strong form given in Eq. (53). The idea is to introduce *new quadrature rules that use CG sites as integration points*. Since we have shown that there exist exact quadratures that use only one point per degree of freedom for Eq. (53), it seems that the weighted residual formulation of the strong form might be more amenable to numerical integration than its weak counterpart. We illustrate this point by considering again the example studied in Sect. 5.1.1. We employ

[3]This statement also holds true for affine geometrical mappings.

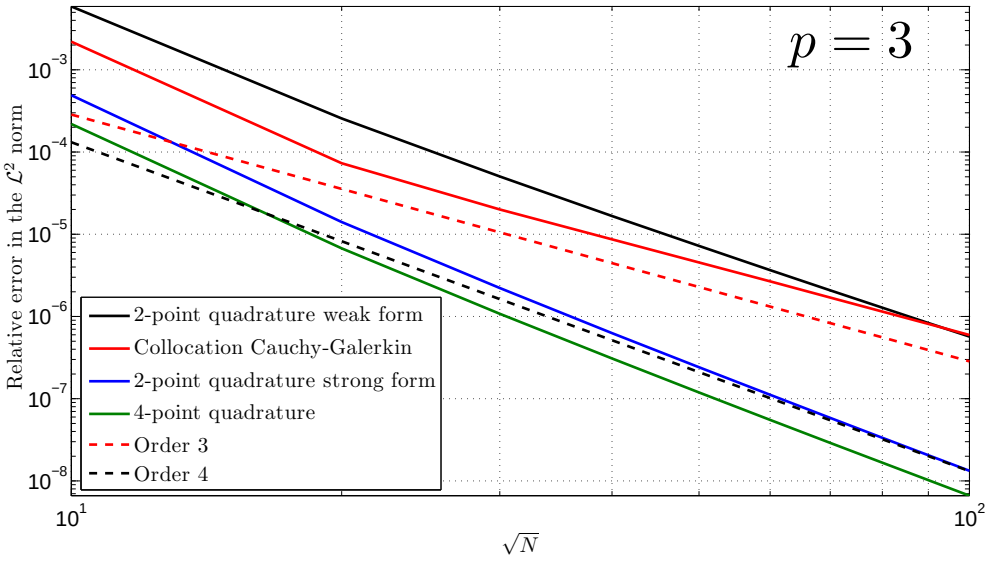

Figure 12: Comparison of several quadrature formulas for the weighted residual formulation of the weak and strong form of a linear elasticity example.

a spline space of degree $p = 3$ in each direction and, unless otherwise stated, we utilize Gauss-Legendre integration on each element. Therefore, standard element-based Gaussian quadrature requires 4 integration points per element in each direction. We solved the problem using: (a) the Galerkin formulation (52) with full integration, i.e., 4 points per element in each direction, (b) the Galerkin formulation (52) with 2 integration points per element in each direction, (c) the weighted residual formulation of the strong form (53) using CG sites as integration points (this leads to 2 integration points per element in each direction), and (d) collocation at CG points. Note that, for the particular case of $p = 3$, the 2-point quadrature rule that uses CG sites as integration points coincides with the 2-point Gauss-Legendre formula, so the integration rules used in cases (b) and (c) are identical, although the integrands are obviously different. Fig. 12 shows the results for all cases. Option (c) clearly outperforms options (b) and (d), which suggests that reduced quadrature rules for the weighted residual formulation of the strong form may be indeed an interesting new method to explore. The fact that (c) outperforms (d) is especially important because it suggests that a new family of schemes may be derived, which outperform collocation at CG points even on the basis of accuracy per computing time.

This idea can be further exploited for other degrees. In some cases, e.g., even degree splines, the use of CG points leads to well-known quadrature formulae, but as far as we are aware, they have not been utilized for Eq. (53). For odd-degree splines, except for $p = 3$, integration at CG points will produce new quadratures, and the standard procedure can be used to determine the proper weights.

7. Conclusions

We proposed the concept of variational collocation as a method for the numerical solution of partial differential equations. The approach shows the potential of achieving the accuracy of variational methods with the computational cost of collocation methods, and is applicable to discretization methods using pointwise non-negative and sufficiently smooth basis functions, prime examples being isogeometric analysis and some meshfree methods (e.g., maximum entropy schemes). This paper focused on isogeometric analysis. We showed that there exists a set of points (denoted as Cauchy-Galerkin points) such that direct collocation of the strong form of the governing partial differential equation at these points produces the Galerkin solution exactly. We then provided both a comprehensive heuristic analysis and a mathematically sound estimate of these points for splines of arbitrary degree and maximum continuity. With examples of linear and non-linear elasticity as well as Kirchhoff plates, we showed that isogeometric collocation at estimated Cauchy-Galerkin points completely solves the well-known odd/even discrepancy in the order of spatial convergence and thus clearly outperforms standard isogeometric collocation. Beyond these already significant results, we believe that variational collocation is a very promising framework to be exploited in several additional problems of computational mechanics.

Acknowledgements

HG was partially supported by the European Research Council through the Starting Grant program (GA 307201). HG also acknowledges the support of the International Research Training Group IRTG 1627, and Xunta de Galicia. LDL was partially supported by the European Research Council through the Starting Grant program (GA 279439), and the DFG Priority Program SPP 1748 "Reliable Simulation Techniques in Solid Mechanics".

Appendix A. Existence of sufficient Cauchy-Galerkin points for isogeometric collocation

The proof of the main theorem follows closely [55, Lemma (38)]. In preparation for the theorem, we recall some basic notions of approximation theory.

Definition 1. Given two functions F and H, and a set of points $\{\gamma_i\}_{i=1,\dots,k+1}$, we will say that the function F *matches* H *in Hermite sense* at $\{\gamma_i\}_{i=1,\dots,k+1}$ if for every site ζ that occurs m times in the sequence $\{\gamma_i\}_{i=1,\dots,k+1}$, F and H verify

$$F^{(j)}(\zeta) = H^{(j)}(\zeta) \quad \text{for} \quad j = 0, \dots, m-1, \tag{A.1}$$

where $F^{(j)}$ denotes the j-th derivative of F.

Definition 2. The *k-th divided difference* of a function F at the points $\{\gamma_i\}_{i=1,\dots,k+1}$, denoted by $\Delta(\gamma_{1:k+1})F$, is the leading coefficient of the polynomial of degree k that matches F in Hermite sense at the set of points $\{\gamma_i\}_{i=1,\dots,k+1}$.

Note that the divided difference is well defined even when there are repeated values in the set $\{\gamma_i\}_{i=1,\dots,k+1}$ because Eq. (A.1) imposes $k+1$ independent conditions irrespectively of the multiplicities of the points. From Definition 2, it is trivial to show that $\Delta(\gamma_{1:1})F = F(\gamma_1)$. When there are no repeated points in the sequence $\{\gamma_i\}_{i=1,\dots,k+1}$ or the repetitions are clustered, divided differences can be also defined recursively. The following statement holds true [56]: Assume that the sequence $\{\gamma_i\}_{i=1,\dots,k+1}$ has all its repeated points (if any) clustered, meaning that, for any $i<j$, $\gamma_i=\gamma_j$ implies that $\gamma_i=\gamma_{i+1}=\cdots=\gamma_j$. Then,

$$\Delta(\gamma_{i:j})F = \begin{cases} \dfrac{\Delta(\gamma_{i+1:j})F - \Delta(\gamma_{i:j-1})F}{\gamma_j-\gamma_i}, & \gamma_i \neq \gamma_j \\ \dfrac{F^{(j-i)}(\gamma_i)}{(j-i)!}, & \gamma_i=\gamma_j \end{cases} \qquad 1\leq i\leq j\leq k+1 \tag{A.2}$$

To prove the main theorem of this Appendix we will also utilize the following Lemma.

Lemma 2 (Peano form of the divided difference)**.** *Let us consider the spline space $\mathcal{S}_{p,\boldsymbol{\Xi}}$ associated to the degree p and the knot vector $\boldsymbol{\Xi}=\{\xi_1,\xi_2,\dots,\xi_{n+p+1}\}$ on the closed interval $[a,b]$. Let $\{N_i\}_{i=1,\dots,n}$ be a basis of $\mathcal{S}_{p,\boldsymbol{\Xi}}$. Then, for any sufficiently smooth function F,*

$$\Delta(\xi_{i:i+p+1})F = \frac{1}{(\xi_{i+p+1}-\xi_i)p!}\int_a^b N_i(s)F^{(p+1)}(s)\mathrm{d}s \quad \textit{for all} \quad i=1,\dots,n \tag{A.3}$$

Proof. The reader is referred to [55] for a proof. □

Theorem 3. *If the knot vector $\boldsymbol{\Xi}=\{\xi_i\}_{i=1,\dots,n+p+1}$ is in the closed interval $[a,b]$ with $\xi_j<\xi_{j+p+1}$ for all $j=1,\dots,n$ (this ensures that the multiplicity of knots is at most $p+1$), and the integrable function $R:[a,b]\mapsto\mathbb{R}$ is orthogonal to the spline space $\mathcal{S}_{p,\boldsymbol{\Xi}}$ on $[a,b]$, that is*

$$\int_a^b s(x)R(x)\mathrm{d}x = 0 \quad \textit{for all} \quad s\in\mathcal{S}_{p,\boldsymbol{\Xi}} \tag{A.4}$$

then, there exists $\boldsymbol{\Lambda}=\{\lambda_1,\lambda_2,\dots,\lambda_{n+1}\}$ in $[a,b]$, strictly increasing with $\xi_i\leq\lambda_i\leq\xi_{i+p}$ (any equality holding only in the trivial case $\xi_i=\xi_{i+p}$) so that R is also orthogonal to $\mathcal{S}_{0,\boldsymbol{\Lambda}}$, that is,

$$\int_{\lambda_i}^{\lambda_{i+1}} R(x)\mathrm{d}x = 0 \quad \textit{for all} \quad i=1,\dots,n. \tag{A.5}$$

Proof. Let us define the function $G:[a,b]\mapsto\mathbb{R}$

$$G(x) = Q(x) + \frac{1}{p!}\int_a^x (x-s)^p R(s)\mathrm{d}s \tag{A.6}$$

where Q is a polynomial of degree p. The polynomial Q can always be taken such that

$$G(\xi_1)=G(\xi_2)=\cdots=G(\xi_{p+1})=0 \tag{A.7}$$

because its $p+1$ coefficients may be determined using the conditions

$$Q(\xi_l) = -\frac{1}{p!}\int_a^{\xi_l} (\xi_l - s)^p R(s)\mathrm{d}s \quad \text{for} \quad l = 1, \ldots, p+1 \tag{A.8}$$

Note that for open knot vectors, Q is identically zero[4]. The derivatives of G, which will be used later, may be computed using Leibniz's rule as

$$\begin{aligned}
G'(x) &= Q'(x) + \frac{1}{(p-1)!}\int_a^x (x-s)^{p-1} R(s)\mathrm{d}s && \text{(A.9)}\\
G''(x) &= Q''(x) + \frac{1}{(p-2)!}\int_a^x (x-s)^{p-2} R(s)\mathrm{d}s && \text{(A.10)}\\
&\vdots \qquad\qquad\qquad\qquad \vdots &&\\
G^{(p)}(x) &= Q^{(p)}(x) + \int_a^x R(s)\mathrm{d}s, \quad \text{where} \quad Q^{(p)} \quad \text{is a constant} && \text{(A.11)}\\
G^{(p+1)}(x) &= R(x) && \text{(A.12)}
\end{aligned}$$

Therefore, if we apply Lemma 2 to the function G and the spline space $\mathcal{S}_{p,\boldsymbol{\Xi}} = \mathrm{span}\{N_i\}_{i=1,\ldots,n}$, we obtain

$$\Delta(\xi_{i:i+p+1})G = \frac{1}{(\xi_{i+p+1} - \xi_i)p!}\int_a^b N_i(s)R(s)\mathrm{d}s \quad \text{for all} \quad i = 1, \ldots, n \tag{A.13}$$

and we know that the right hand side of Eq. (A.13) vanishes due to the assumption (A.4) and the obvious fact that $N_i \in \mathcal{S}_{p,\boldsymbol{\Xi}}$. Then, we conclude

$$\Delta(\xi_{i:i+p+1})G = 0 \quad \text{for all} \quad i = 1, \ldots, n \tag{A.14}$$

Let us focus on Eq. (A.14) for $i = 1$. We know that Eq. (A.7) holds and the recursive definition of the divided difference may be used to show that $G(\xi_{p+2}) = 0$. This argument may be applied recurrently to show that G vanishes at all knots. If there are repeated knots in $\boldsymbol{\Xi}$, then some derivatives of G can also be proven to be zero at the repeated knots, but this is not needed for the proof.

We could now use Rolle's theorem to show the existence of the set of points $\{\eta_1, \eta_2, \ldots, \eta_{n+p}\}$ such that $G'(\eta_i) = 0$ with $\eta_i \in (\xi_i, \xi_{i+1})$ for all $i = 1, \ldots, n+p$. If we apply the same argument again, we may prove the existence of the set $\{\mu_1, \mu_2, \ldots, \mu_{n+p-1}\}$ such that

$$G''(\mu_i) = 0 \quad \text{with} \quad \mu_i \in (\xi_i, \xi_{i+2}),\ i = 1, \ldots, n+p-1 \tag{A.15}$$

Using Rolle's theorem recursively, we can show the existence of $\{\lambda_1, \lambda_2, \ldots, \lambda_{n+1}\}$ such that

$$G^{(p)}(\lambda_i) = 0 \quad \text{with} \quad \lambda_i \in (\xi_i, \xi_{i+p}),\ i = 1, \ldots, n+1 \tag{A.16}$$

[4]Note that in many cases of practical relevance, Q might not be zero because some functions in the spline space are not used to enforce Eq. (A.4), but to impose Dirichlet boundary conditions.

Now, utilizing Eq. (A.11) repeatedly at the λ_i's, it follows trivially that

$$\int_{\lambda_i}^{\lambda_{i+1}} R(s)\mathrm{d}s = 0 \quad \text{for} \quad i = 1, \ldots, n \tag{A.17}$$

which shows that R is orthogonal to $\mathcal{S}_{0,\mathbf{\Lambda}}$ and concludes the proof. □

Corollary 3.1. *If R is continuous, then there exists the set $\boldsymbol{\tau} = \{\tau_1, \tau_2, \ldots, \tau_n\}$, strictly increasing, with $\tau_i \in (\xi_i, \xi_{i+p+1})$ for all $i = 1, \ldots, n$, such that*

$$R(\tau_i) = 0, \quad i = 1, \ldots, n \tag{A.18}$$

Proof. The result follows trivially from the application of the mean value theorem of integral calculus to Eq. (A.17). □

Final result: If we apply Theorem 3, and Corollary 3.1 to Eq. (10) with $\Omega = [a, b]$, it follows directly that there exist at least n distinct CG points for a space of dimension n. Collocation at those points produces the Galerkin solution exactly.

Appendix B. Heuristic study of the location of Cauchy-Galerkin points

This Appendix follows up on Sect. 4.2. We study heuristically the location of CG points for different forcing functions and for various degrees of the spline space. Our model problem is

$$u'' + f = 0 \quad \text{in} \quad x \in (0, 1) \tag{B.1}$$

$$u(0) = u(1) = 0 \tag{B.2}$$

with $f(x) = -p_w(p_w - 1)x^{p_w - 2}$ and $u(x) = x^{p_w} - x$. We always take $p_w > p$, where p is the degree of the splines, so that the Galerkin solution is not exact. In all cases we take uniform knot vectors, although the results carried on in the cases with non-uniform knot vectors that we computed.

Appendix B.1. Cauchy-Galerkin points for splines of odd degree

We studied spline spaces of degree $p = 3$, $p = 5$, $p = 7$ and $p = 9$, but we only show here $p = 3$ and $p = 5$ for conciseness. The cases with odd degree and $p > 5$ behaved very similarly to $p = 3$ and $p = 5$. Fig. B.13 shows a rescaled plot of R_h for a cubic spline space with a uniform knot vector and $n = 30$. We use the forcing given by $p_w = 4$ (blue), $p_w = 5$ (red) and $p_w = 6$ (green). Again, Greville points seem to be the worst possible choice for all forcing functions. It may also be observed that, irrespectively of the forcing, there are approximately two CG points per knot span. These points are symmetrically distributed over the knot span and the offset with respect to knots is markedly constant. The location of the points coincides with the theoretical prediction given in Eq. (37). Fig. B.14 shows the same information as Fig. B.13, but now using $p = 5$ and with the polynomial forcing defined by $p_w = 6$ (blue), $p_w = 7$ (red) and $p_w = 8$ (green). The pattern is almost identical, but the offset with respect to knots is slightly different. A quantitative study of the location of the points suggested that they fall at the positions given in Tab. C.3. All these trends remained for larger values of n.

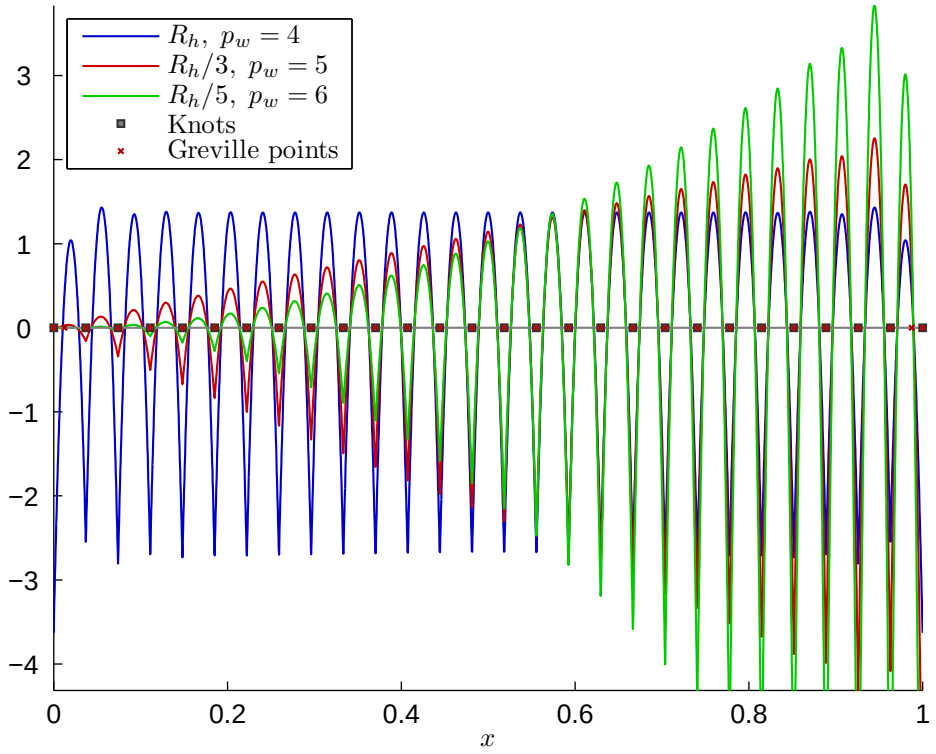

Figure B.13: CG points for the one-dimensional Poisson equation. The spline space is defined by a uniform, open knot vector and $n = 30$, $p = 3$. We use the polynomial forcing $f(x) = -p_w(p_w - 1)x^{p_w - 2}$ with $p_w = 4$, $p_w = 5$ and $p_w = 6$.

Appendix B.2. Cauchy-Galerkin points for splines of even degree

We studied the cases $p = 2$, $p = 4$, $p = 6$ and $p = 8$, but we only show here $p = 2$ and $p = 4$ for conciseness. The cases with even degree greater than 4 behave very similarly to the case $p = 4$. We start by emphasizing that the case $p = 2$ is special and actually Corollary 3.1 does not apply for $p = 2$ because the function $R_h = u_h'' - f$ is discontinuous. However, in all the cases that we computed we always found enough CG points to perform variational collocation. Fig. B.15 shows the results using a uniform and open knot vector with $n = 30$. The forcing function is defined by $p_w = 3$ (blue), $p_w = 4$ (red) and $p_w = 5$ (green). Essentially, CG points fall on top of Greville points as predicted by the theory (cf. Tab. C.2). Fig. B.16 shows the results for quartic splines and the forcings given by $p_w = 5$ (blue), $p_w = 6$ (red) and $p_w = 7$ (green). As in the odd-degree case, there seems to be roughly two families of CG points, but in this case, one family falls on top of Greville points and another one on top of knots. The results confirm again the theoretical predictions.

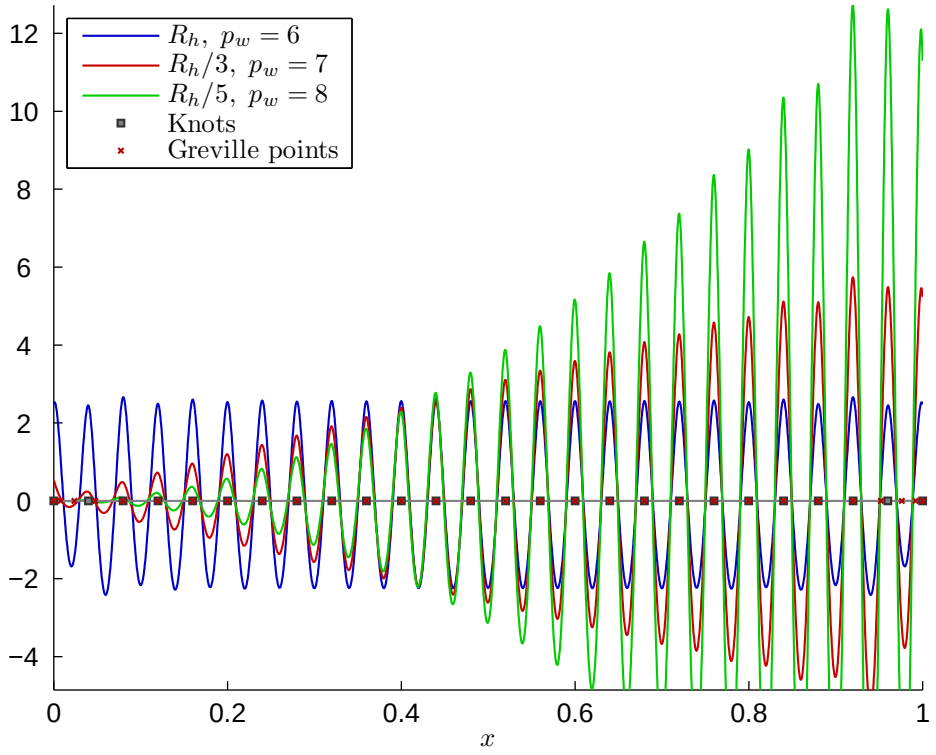

Figure B.14: CG points for the one-dimensional Poisson equation. The spline space is defined by a uniform, open knot vector and $n = 30$, $p = 5$. We use the polynomial forcing $f(x) = -p_w(p_w - 1)x^{p_w - 2}$ with $p_w = 6$, $p_w = 7$ and $p_w = 8$.

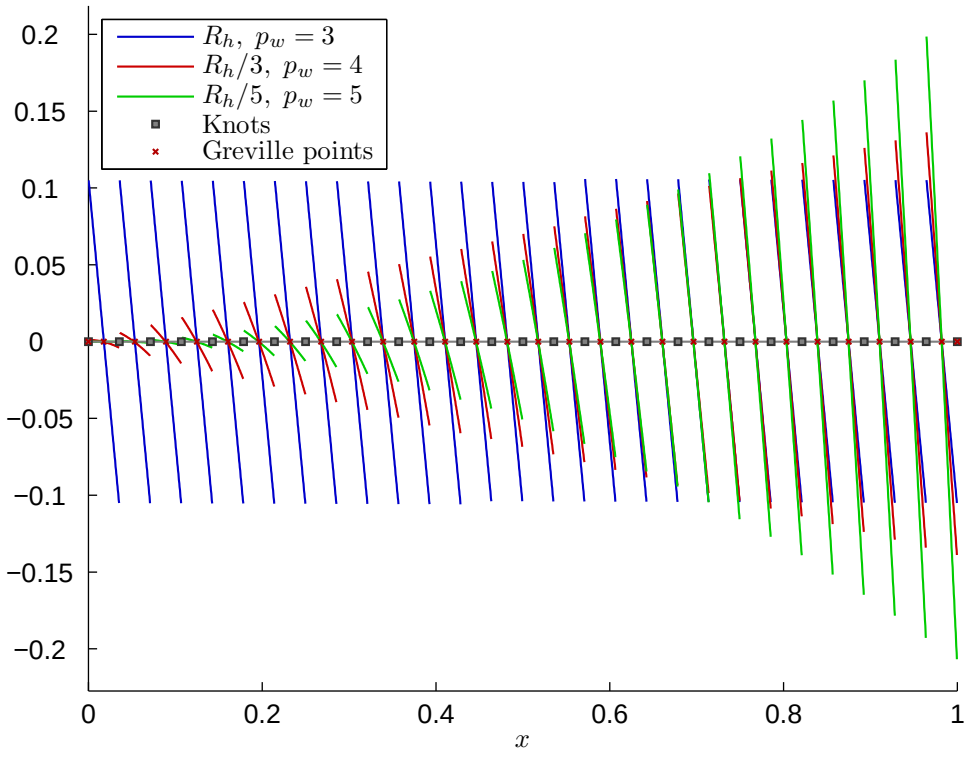

Figure B.15: CG points for the one-dimensional Poisson equation. The spline space is defined by a uniform, open knot vector and $n = 30$, $p = 2$. We use the polynomial forcing $f(x) = -p_w(p_w - 1)x^{p_w - 2}$ with $p_w = 3$, $p_w = 4$ and $p_w = 5$.

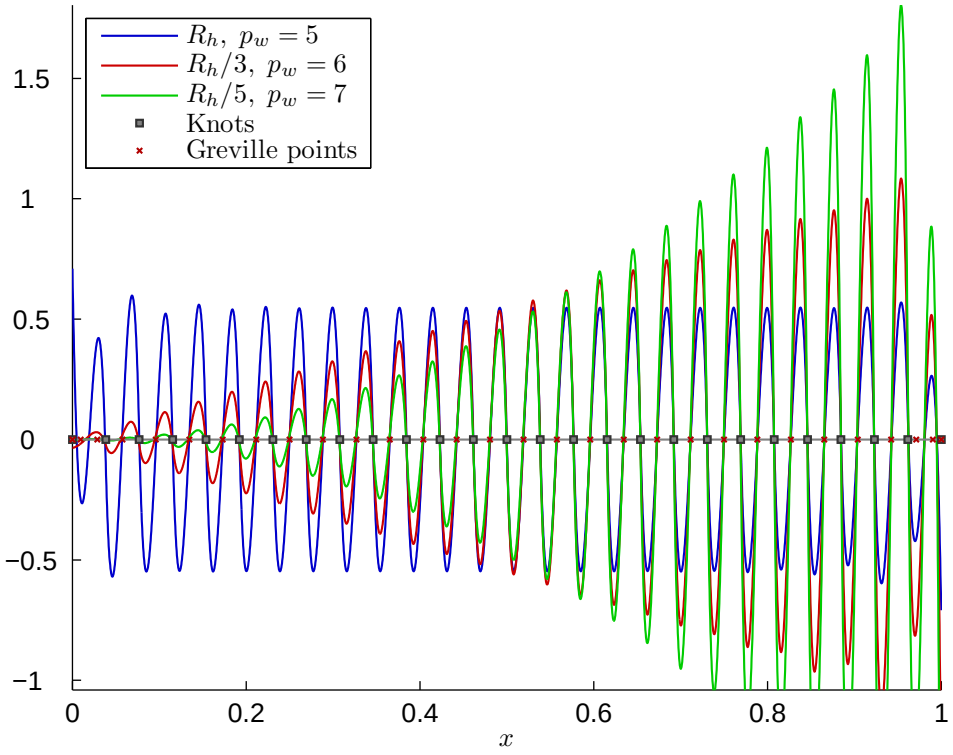

Figure B.16: CG points for the one-dimensional Poisson equation. The spline space is defined by a uniform, open knot vector and $n = 30$, $p = 4$. We use the polynomial forcing $f(x) = -p_w(p_w - 1)x^{p_w - 2}$ with $p_w = 5$, $p_w = 6$ and $p_w = 7$.

Appendix C. Location of Cauchy-Galerkin points based on the superconvergence theory

As follows, we propose a general method to find the CG points for splines of order p and maximum continuity $\mu = p - 1$. We also introduce $r = p + 1$.

As illustrated in Sect. 4.3 for $p = 3$, in order to find the points it is first necessary to perform a Taylor expansion of the error $e = u - u_h$ up to order $r = 4$ within two adjacent knot spans around their respective midpoints, and to find for each knot span the $r + 1$ coefficients in the expansion up to a scaling factor. This implies imposing a total number of conditions equal to $2\,(r + 1) - 1 = 9$. What these conditions are has been already detailed in Sect. 4.3. Following the same reasoning for splines of arbitrary order and maximum continuity, the expansion of the error must be performed within a suitable number of knot spans n_s around their respective midpoints, with n_s chosen in such a way that the total number of equations available to find the coefficients be $n_s\,(r + 1) - 1$. These equations stem from (a) the known conditions on superconvergence of e (for even p) or of e' (for odd p) at knots and midpoints [47]; (b) the continuity conditions of e and its derivatives up to order μ at the knots; (c) weighted residual conditions of the type of Eq. (28) written using as weighting functions all the splines of degree $p-2$ having full support on the n_s considered knot spans. The above procedure becomes increasingly cumbersome as p increases. For this reason, we propose henceforth an alternative method which is significantly simpler, yet rigorous, and which delivers identical results to the aforementioned procedure. The method is based on the *a priori* assumption that the coefficients of the error expansion are the same in each knot span, so that the expansion reads

$$e = c_0 P_0 + c_1 P_1 + ... + c_r P_r + R \qquad \text{in } [-1, 1] \tag{C.1}$$

with $R = \mathcal{O}\,(h^{r+1})$ as the remainder. Here P_m denotes the Legendre polynomial of degree m on the normalized domain $[-1, 1]$, and c_m is the corresponding coefficient in the Taylor expansion. As follows, we list the conditions available and illustrate the strategy to find the unknown coefficients $c_0, ..., c_r$ up to a scaling factor for the cases of even and odd p. Note that the aforementioned *a priori* assumption can be verified *a posteriori*, so that the found solution is certainly exact.

Appendix C.1. Finding the points for even p

For even p, it is known [47] that e is superconvergent at the knots and at the midpoint of each knot span. The superconvergence conditions at the knots of the (generic normalized) knot span under consideration read $e\,(-1) = e\,(+1) = \mathcal{O}\,(h^{r+1})$ and lead to the following two equations

$$c_0 + c_2 + ... + c_{r-1} = \mathcal{O}\left(h^{r+1}\right) \tag{C.2}$$

$$c_1 + c_3 + ... + c_r = \mathcal{O}\left(h^{r+1}\right) \tag{C.3}$$

Furthermore, the superconvergence condition on e at the midpoint, $e\,(0) = \mathcal{O}\,(h^{r+1})$, gives

$$c_0 P_0(0) + c_2 P_2(0) + ... + c_{r-1} P_{r-1}(0) = \mathcal{O}\left(h^{r+1}\right) \tag{C.4}$$

The second set of conditions is related to continuity. Being e automatically continuous as a result of the superconvergence conditions at the knots, continuity needs to be enforced for e', e'' and all the subsequent derivatives up to the order $\mu = p-1 = r-2$. E.g., continuity of e' leads to $e'(1) - e'(-1) = \mathcal{O}(h^r)$, and thus to

$$c_2 P_2'(1) + c_4 P_4'(1) + ... + c_{r-1} P_{r-1}'(1) = \mathcal{O}\left(h^{r+1}\right) \tag{C.5}$$

Continuity of e'' leads to

$$c_3 P_3''(1) + c_5 P_5''(1) + ... + c_r P_r''(1) = \mathcal{O}\left(h^{r+1}\right) \tag{C.6}$$

We can further enforce continuity of all derivatives up to $e^{(p-1)} = e^{(r-2)}$, this last condition yielding

$$c_{r-1} = \mathcal{O}\left(h^{r+1}\right) \tag{C.7}$$

Eq. (C.7), in combination with continuity conditions of the odd derivatives e', e''', ..., $e^{(r-4)}$ and with Eq. (C.4), gives

$$c_0 = c_2 = ... = c_{r-1} = \mathcal{O}\left(h^{r+1}\right) \tag{C.8}$$

which eliminates all terms with even index from the expansion (C.1). As a result, Eq. (C.2) becomes a redundant identity. We are thus left with Eq. (C.3), and all continuity conditions of the even derivatives e'', $e^{(4)}, ..., e^{(r-3)}$. This is a reduced set of $n_{eq} = 1 + \frac{r-3}{2} = \frac{r-1}{2}$ equations, in the reduced set of unknowns $n_{unk} = \frac{r+1}{2}$. As desired, it is thus $n_{eq} = n_{unk} - 1$, with no need to exploit weighted residual conditions such as in the general procedure outlined earlier. The condition on the continuity of $e^{(r-3)}$ reads

$$c_{r-2} P_{r-2}^{(r-3)}(1) + c_r P_r^{(r-3)}(1) = \mathcal{O}\left(h^{r+1}\right) \tag{C.9}$$

from which we obtain, to leading order,

$$c_{r-2} = -\frac{P_r^{(r-3)}(1)}{P_{r-2}^{(r-3)}(1)} c_r \tag{C.10}$$

The condition on the continuity of $e^{(r-5)}$ leads to

$$c_{r-4} P_{r-4}^{(r-5)}(1) + c_{r-2} P_{r-2}^{(r-5)}(1) + c_r P_r^{(r-5)}(1) = \mathcal{O}\left(h^{r+1}\right) \tag{C.11}$$

which can be combined with Eq. (C.10) to express also c_{r-4} as a function of c_r. Proceeding with the remaining continuity conditions of the even derivatives, all other coefficients with even index can be computed as functions of c_r.

Appendix C.2. Finding the points for odd p

For odd p, it is known [47] that e' is superconvergent at the knots and at the midpoint of each knot span. The superconvergence conditions at the knots read $e'(-1) = e'(+1) = \mathcal{O}(h^r)$ and lead to the following two equations

$$c_1 + c_3 P_3'(1) + ... + c_{r-1} P_{r-1}'(1) = \mathcal{O}\left(h^{r+1}\right) \tag{C.12}$$

$$c_2 P_2'(1) + c_4 P_4'(1) + ... + c_r P_r'(1) = \mathcal{O}\left(h^{r+1}\right) \tag{C.13}$$

Furthermore, the superconvergence condition on e' at the midpoint, $e'(0) = \mathcal{O}(h^r)$, gives

$$c_1 + c_3 P_3'(0) + ... + c_{r-1} P_{r-1}'(0) = \mathcal{O}\left(h^{r+1}\right) \tag{C.14}$$

Also in this case the second set of conditions stems from continuity. Being e' automatically continuous as a result of the superconvergence conditions at the knots, continuity needs to be enforced for e, e'' and all the subsequent derivatives up to the order $\mu = p - 1 = r - 2$. Continuity of e leads to $e(1) - e(-1) = \mathcal{O}(h^r)$, and thus to

$$c_1 + c_3 + ... + c_{r-1} = \mathcal{O}\left(h^{r+1}\right) \tag{C.15}$$

Continuity of e'' yields

$$c_3 P_3''(1) + c_5 P_5''(1) + ... + c_{r-1} P_{r-1}''(1) = \mathcal{O}\left(h^{r+1}\right) \tag{C.16}$$

We can further enforce continuity of all derivatives up to $e^{(p-1)} = e^{(r-2)}$, this last condition yielding

$$c_{r-1} = \mathcal{O}\left(h^{r+1}\right) \tag{C.17}$$

Eq. (C.17), in combination with continuity conditions of e and of its even derivatives $e'', ..., e^{(r-4)}$, gives

$$c_1 = c_3 = ... = c_{r-1} = \mathcal{O}\left(h^{r+1}\right) \tag{C.18}$$

which eliminates all terms with odd index from the expansion (C.1). As a result, Eqns. (C.12) and (C.14) become redundant identities. We are thus left with Eq. (C.13), and all continuity conditions of the odd derivatives $e''', ..., e^{(r-3)}$. This is a reduced set of $n_{eq} = 1 + \frac{r-4}{2} = \frac{r-2}{2}$ equations, in the reduced set of unknowns $n_{unk} = \frac{r+2}{2}$. In this case it is thus $n_{eq} = n_{unk} - 2$. However, using a weighted residual condition it can be proven that $c_0 = 0$. We omit this proof as we are only interested in the derivatives of the error, for which the term with coefficient c_0 does not play any role. The condition on the continuity of $e^{(r-3)}$ leads as before to

$$c_{r-2} = -\frac{P_r^{(r-3)}(1)}{P_{r-2}^{(r-3)}(1)} c_r, \tag{C.19}$$

which holds to leading order. Once again we can proceed in using the remaining continuity conditions of the odd derivatives to express all other coefficients with odd index as functions of c_r.

p	$e_R(\eta)$	$e''_R(\eta)$
2	$\eta^3 - \eta$	η
3	$15\eta^4 - 30\eta^2 + 7$	$3\eta^2 - 1$
4	$3\eta^5 - 10\eta^3 + 7\eta$	$\eta^3 - \eta$
5	$21\eta^6 - 105\eta^4 + 147\eta^2 - 31$	$15\eta^4 - 30\eta^2 + 7$
6	$3\eta^7 - 21\eta^5 + 49\eta^3 - 31\eta$	$3\eta^5 - 10\eta^3 + 7\eta$
7	$15\eta^8 - 140\eta^6 + 490\eta^4 - 620\eta^2 + 127$	$21\eta^6 - 105\eta^4 + 147\eta^2 - 31$

Table C.2: Error functions and their second and fourth derivatives for different interpolation degrees.

p	Zeros of e''
3	$\pm\frac{1}{\sqrt{3}}$
5	$\pm\frac{\sqrt{225-30\sqrt{30}}}{15}$
7	± 0.5049185675126533

Table C.3: CG points for different interpolation degrees.

Appendix C.3. Summary of results

We summarize the results of the procedure outlined above, in terms of the rescaled error function e_R and of its second derivative, in Table C.2. The zeros of the second derivative for even degrees, as expected, coincide with the knots and midpoint of the knot span. The same zeros for odd degrees are summarized in Table C.3 and represent the sought CG points.

[1] C. Canuto, M. Y. Hussaini, A. M. Quarteroni, T. A. Zang, Spectral methods. Fundamentals in single domains, Springer Science & Business Media, 2006.

[2] A. Quarteroni, A. Valli, Numerical approximation of partial differential equations, Vol. 23, Springer, 2008.

[3] D. Schillinger, J. A. Evans, F. Frischmann, R. R. Hiemstra, M.-C. Hsu, T. J. Hughes, A collocated c0 finite element method: Reduced quadrature perspective, cost comparison with standard finite elements, and explicit structural dynamics, International Journal for Numerical Methods in Engineering 102 (3-4) (2015) 576–631.

[4] T. J. R. Hughes, J. A. Cottrell, Y. Bazilevs, Isogeometric analysis CAD, finite elements, NURBS, exact geometry and mesh refinement, Computacional Methods in Applied Mechanics and Engineering 194 (2005) 4135–4195.

[5] J. A. Cottrell, T. J. R. Hughes, Y. Bazilevs, Isogeometric Analysis Toward Integration of CAD and FEA, Wiley, 2009.

[6] Y. Bazilevs, V. Calo, J. Cottrell, J. Evans, T. Hughes, S. Lipton, M. Scott, T. Sederberg, Isogeometric analysis using T-splines, Computer Methods in Applied Mechanics and Engineering 199 (2010) 229–263.

[7] H. Gomez, V. M. Calo, Y. Bazilevs, T. J. R. Hughes, Isogeometric analysis of the Cahn-Hilliard phase-field model, Computer Methods in Applied Mechanics and Engineering 197 (49-50) (2008) 4333–4352.

[8] H. Gomez, T. J. Hughes, X. Nogueira, V. M. Calo, Isogeometric analysis of the isothermal Navier–Stokes–Korteweg equations, Computer Methods in Applied Mechanics and Engineering 199 (2010) 1828–1840.

[9] S. Lipton, J. Evans, Y. Bazilevs, T. Elguedj, T. J. R. Hughes, Robustness of isogeometric structural discretizations under severe mesh distortion, Computer Methods in Applied Mechanics and Engineering 199 (2010) 357–373.

[10] J. A. Evans, T. J. Hughes, Isogeometric divergence-conforming B-splines for the unsteady Navier–Stokes equations, Journal of Computational Physics 241 (2013) 141–167.

[11] F. Auricchio, L. Da Veiga, T. J. R. Hughes., A. Reali, G. Sangalli, Isogeometric collocation methods, Mathematical Models and Methods in Applied Sciences 20 (2010) 2075–2107.

[12] F. Auricchio, L. B. da Veiga, T. Hughes, A. Reali, G. Sangalli, Isogeometric collocation for elastostatics and explicit dynamics, Computer Methods in Applied Mechanics and Engineering 249 (2012) 2–14.

[13] H. Casquero, L. Liu, Y. Zhang, A. Reali, H. Gomez, Isogeometric collocation using analysis-suitable t-splines of arbitrary degree, Computer Methods in Applied Mechanics and Engineering 301 (2016) 164 – 186.

[14] H. Gomez, A. Reali, G. Sangalli, Accurate, efficient, and (iso)geometrically flexible collocation methods for phase-field models, Journal of Computational Physics 262 (2014) 153–171.

[15] A. Reali, H. Gomez, An isogeometric collocation approach for Bernoulli-Euler beams and kirchhoff plates, Computer Methods in Applied Mechanics and Engineering 284 (2015) 623–636.

[16] H. Casquero, L. Liu, C. Bona-Casas, Y. Zhang, H. Gomez, A hybrid variational-collocation immersed method for fluid-structure interaction using unstructured T-splines, International Journal for Numerical Methods in Engineering.

[17] L. De Lorenzis, J. Evans, T. Hughes, A. Reali, Isogeometric collocation: Neumann boundary conditions and contact, Computer Methods in Applied Mechanics and Engineering 284 (2015) 21–54.

[18] R. Kruse, N. Nguyen-Thanh, L. De Lorenzis, T. Hughes, Isogeometric collocation for large deformation elasticity and frictional contact problems, Computer Methods in Applied Mechanics and Engineering 296 (2015) 73–112.

[19] D. Schillinger, J. Evans, A. Reali, M. Scott, T. J. R. Hughes, Isogeometric collocation: Cost comparison with Galerkin methods and extension to adaptive hierarchical NURBS discretizations, Computer Methods in Applied Mechanics and Engineering 267 (2013) 170–232.

[20] E. W. Hobson, The Theory of Functions of A Real Variable and The Theory of Fourier's Series., 1907.

[21] T. J. R. Hughes, The Finite Element Method: Linear Static and Dynamic Finite Element AnalysisCited By (since 1996)1023.

[22] S. Li, W. K. Liu, Meshfree particle methods, Springer Science & Business Media, 2007.

[23] M. Arroyo, M. Ortiz, Local maximum-entropy approximation schemes: a seamless bridge between finite elements and meshfree methods, International journal for numerical methods in engineering 65 (13) (2006) 2167–2202.

[24] J. Kiendl, K.-U. Bletzinger, J. Linhard, R. Wuchner, Isogeometric shell analysis with Kirchhoff-Love elements, Computer Methods in Applied Mechanics and Engineering 198 (2009) 3902–3914.

[25] T. Elguedj, Y. Bazilevs, V. M. Calo, T. J. Hughes, $\overline{B}$ and $\overline{F}$ projection methods for nearly incompressible linear and non-linear elasticity and plasticity using higher-order NURBS elements, Computer methods in applied mechanics and engineering 197 (2008) 2732–2762.

[26] F. Auricchio, L. B. da Veiga, A. Buffa, C. Lovadina, A. Reali, G. Sangalli, A fully "locking-free" isogeometric approach for plane linear elasticity problems: a stream function formulation, Computer methods in applied mechanics and engineering 197 (1) (2007) 160–172.

[27] R. Dimitri, L. De Lorenzis, P. Wriggers, G. Zavarise, NURBS and T-spline-based isogeometric cohesive zone modeling of interface debonding, Computational Mechanics 54 (2) (2014) 369–388.

[28] R. Dhote, H. Gomez, R. Melnik, J. Zu, Shape memory alloy nanostructures with coupled dynamic thermo-mechanical effects, Computer Physics Communications (0) (2015) –.

[29] R. Dhote, H. Gomez, R. Melnik, J. Zu, Isogeometric analysis of a dynamic thermo-mechanical phase-field model applied to shape memory alloys, Computational Mechanics 53 (2013) 1235–1250.

[30] Y. Bazilevs, V. M. Calo, J. A. Cottrell., T. J. R. Hughes, A. Reali, G. Scovazzi, Variational multiscale residual-based turbulence modeling for large eddy simulation of incompressible flows, Computer Methods in Applied Mechanics and Engineering 197 (2007) 173–201.

[31] H. Gomez, L. Cueto-Felgueroso, R. Juanes, Three-dimensional simulation of unstable gravity-driven infiltration of water into a porous medium, Journal of Computational Physics 238 (2013) 217–239.

[32] J. Liu, C. M. Landis, H. Gomez, T. J. Hughes, Liquid–vapor phase transition: Thermomechanical theory, entropy stable numerical formulation, and boiling simulations, Computer Methods in Applied Mechanics and Engineering 297 (2015) 476–553.

[33] M. Ambati, T. Gerasimov, L. De Lorenzis, A review on phase-field models of brittle fracture and a new fast hybrid formulation, Computational Mechanics 55 (2) (2015) 383–405.

[34] H. Gomez, X. Nogueira, An unconditionally energy-stable method for the phase field crystal equation, Computer Methods in Applied Mechanics and Engineering 249 (2012) 52–61.

[35] J. Liu, H. Gomez, J. A. Evans, T. J. Hughes, C. M. Landis, Functional entropy variables: a new methodology for deriving thermodynamically consistent algorithms for complex fluids, with particular reference to the isothermal Navier-Stokes-Korteweg equations, Journal of Computational Physics 248 (2013) 47–86.

[36] R. Dimitri, L. De Lorenzis, M. Scott, P. Wriggers, R. Taylor, G. Zavarise, Isogeometric large deformation frictionless contact using t-splines, Computer methods in applied mechanics and engineering 269 (2014) 394–414.

[37] L. De Lorenzis, P. Wriggers, G. Zavarise, A mortar formulation for 3D large deformation contact using NURBS-based isogeometric analysis and the augmented Lagrangian method, Computational Mechanics 49 (1) (2012) 1–20.

[38] G. Vilanova, I. Colominas, H. Gomez, Capillary networks in tumor angiogenesis: From discrete endothelial cells to phase-field averaged descriptions via isogeometric analysis, International Journal for Numerical Methods in Biomedical Engineering 29 (2013) 1015–1037.

[39] G. Vilanova, I. Colominas, H. Gomez, Coupling of discrete random walks and continuous modeling for three-dimensional tumor-induced angiogenesis, Computational Mechanics 53 (2013) 449–464.

[40] Y. Bazilevs, V. M. Calo, T. J. R. Hughes, Y. Zhang, Isogeometric fluid-structure interaction: Theory, algorithms, and computations, Computational Mechanics 43 (2008) 3–37.

[41] D. Kamensky, M.-C. Hsu, D. Schillinger, J. A. Evans, A. Aggarwal, Y. Bazilevs, M. S. Sacks, T. J. Hughes, An immersogeometric variational framework for fluid-structure interaction: Application to bioprosthetic heart valves, Computer Methods in Applied Mechanics and Engineering 284 (2015) 1005–1053.

[42] J. Bueno, C. Bona-Casas, Y. Bazilevs, H. Gomez, Interaction of complex fluids and solids: theory, algorithms and application to phase-change-driven implosion, Computational Mechanics (2014) 1–14.

[43] H. Casquero, C. Bona-Casas, H. Gomez, A NURBS-based immersed methodology for fluid-structure interaction, Computer Methods in Applied Mechanics and Engineering 284 (2015) 943–970.

[44] I. Babuška, T. Strouboulis, C. Upadhyay, S. Gangaraj, Computer-based proof of the existence of superconvergence points in the finite element method; superconvergence of the derivatives in finite element solutions of Laplace's, Poisson's, and the elasticity equations, Numerical Methods for Partial Differential Equations 12 (3) (1996) 347–392.

[45] J. Barlow, Optimal stress locations in finite element models, International Journal for Numerical Methods in Engineering 10 (2) (1976) 243–251.

[46] I. Babuška, U. Banerjee, J. E. Osborn, Superconvergence in the generalized finite element method, Numerische Mathematik 107 (3) (2007) 353–395.

[47] L. B. Wahlbin, Superconvergence in Galerkin finite element methods, Springer, 1995.

[48] C. Anitescu, Y. Jia, Y. J. Zhang, T. Rabczuk, An isogeometric collocation method using superconvergent points, Computer Methods in Applied Mechanics and Engineering 284 (2015) 1073–1097.

[49] Y. Bazilevs, V. Calo, J. Cottrell, J. Evans, T. Hughes, S. Lipton, M. Scott, T. Sederberg, Isogeometric analysis using t-splines, Computer Methods in Applied Mechanics and Engineering 199 (5-8) (2010) 229–263.

[50] L. Beirao da Veiga, A. Buffa, G. Sangalli, R. Vázquez, Analysis suitable T-splines of arbitrary degree: Definition, linear independence, and approximation properties, Mathematical Models and Methods in Applied Sciences 23 (11) (2013) 1979–2003.

[51] J. Simo, K. Pister, Remarks on rate constitutive equations for finite deformation 46 (1984) 201–215.

[52] A. Reali, H. Gomez, An isogeometric collocation approach for Bernoulli-Euler beams and Kirchhoff plates, Computer Methods in Applied Mechanics and Engineering 284 (2015) 623–636.

[53] D. Schillinger, S. J. Hossain, T. J. Hughes, Reduced bézier element quadrature rules for quadratic and cubic splines in isogeometric analysis, Computer Methods in Applied Mechanics and Engineering 277 (2014) 1 – 45.

[54] T. Hughes, A. Reali, G. Sangalli, Efficient quadrature for nurbs-based isogeometric analysis, Computer Methods in Applied Mechanics and Engineering 199 (5–8) (2010) 301 – 313, computational Geometry and Analysis.

[55] C. De Boor, A practical guide to splines, Mathematics of Computation.

[56] C. de Boor, Divided differences, Surv. Approx. Theory 1 (2005) 46–69.